Valve-less Diffuser Micropumps

Anders Olsson

Instrumentation Laboratory
Department of Signals, Sensors and Systems
Royal Institute of Technology

TRITA-ILA-9803
ISSN 0281-2878

Submitted to the School of Electrical Engineering, Royal Institute of Technology, in partial fulfillment of the requirements for the degree of Doctor of Philosophy.

Stockholm 1998

The front cover shows a photo of the glass side of an 80 μm deep deep reactive ion etched (DRIE) diffuser pump. The size of the pump chip is 15×17×1 mm, the pump chamber diameter is 6 mm and the smallest diffuser dimension is 80 μm. (Photo: TS Mediateknik)

Copyright © 1998 by Anders Olsson

Printed by KTH Högskoletryckeriet, Stockholm 1998

Thesis for the degree of Doctor of Philosophy at the Royal Institute of Technology, 1998.

Abstract

Today there is growing interest in research on microfluidic systems, e.g., for chemical analysis systems and microdosage systems. One of the basic components in microfluidic systems is micropumps. During recent years several different micropumps have been presented based on different pump principles and using different actuation principles. In this thesis the first micromachined versions of pumps based on the new valve-less diffuser pump principle are presented.

The key element in the diffuser pump is the diffuser element. A diffuser is a gradually expanding flow channel intended to raise the static pressure. The largest pressure rise is achieved for small opening angles. The diffuser element is a diffuser with a rounded inlet and a sharp outlet. It is characterized by a lower flow resistance in the diffuser direction than in the opposite direction, the nozzle direction.

In the valve-less diffuser pump diffuser elements are used as flow directing elements. One diffuser element is directed from the inlet chamber to the pump chamber and the other diffuser element from the pump chamber to the outlet chamber. A moving boundary of the pump chamber forces the fluid through the two diffuser elements. The result is a net transport of fluid from the inlet side to the outlet side due to the difference in the flow resistances in the diffuser and nozzle directions.

Pumps of different sizes for both liquids and gases have been fabricated in different materials using both conventional fabrication methods and micromachining technology. Extensive measurements have been made to investigate the performance of the diffuser pumps. These results have been used together with numerical simulations and classical fluid mechanics in order to understand the working principle of the diffuser pump and to further improve the design. Based on the empirical results and simulations using a lumped-mass model improved designs are suggested.

All the tested pumps show good performance. The pump with the best test result is fabricated in silicon using deep reactive ion etching (DRIE) which allows any arbitrary planar design of the pump. A glass wafer is bonded to the pump cavity side of the silicon wafer. The pump diaphragms are excited using piezoelectric discs. The diffuser "throat" cross-section is 80×80 μm and the pump chamber diameter is 6 mm. The entire pump chip has a size of 15×17×1 mm. For water a maximum pressure head of 74 kPa was reached and a maximum volume flow of 2.3 ml/min was obtained.

Anders Olsson, Instrumentation Laboratory, Department of Signals, Sensors and Systems, Royal Institute of Technology, SE-100 44 Stockholm, Sweden.

To my Parents

”I devoted myself to study and to explore by wisdom all that is done under heaven. What a heavy burden God has laid on men!”
Ecclesiastes 1:13

”Be warned, my son, of anything in addition to them. Of making many books there is no end, and much study wearies the body.”
Ecclesiastes 12:12

Scripture quotations are from the Holy Bible, New International Version.
Copyright © 1973, 1978, 1984 by International Bible Society.
Published by Zondervan and Hodder & Stoughton.

This presented thesis is based on the following eight papers:

1 **A valve-less planar fluid pump with two pump chambers**
Anders Olsson, Göran Stemme and Erik Stemme
Sensors and Actuators A 46-47 (1995) 549-556.

2 **A valve-less planar pump isotropically etched in silicon**
Anders Olsson, Peter Enoksson, Göran Stemme and Erik Stemme
Journal of Micromechanics and Microengineering 6 (1996) 87-91.

3 **Diffuser-element design investigation for valve-less pumps**
Anders Olsson, Göran Stemme and Erik Stemme
Sensors and Actuators A 57 (1996) 137-143.

4 **Micromachined flat-walled valve-less diffuser pumps**
Anders Olsson, Peter Enoksson, Göran Stemme and Erik Stemme
Journal of Microelectromechanical Systems, Vol. 6, No. 2, June 1997, 161-166

5 **Valve-less diffuser micropumps fabricated using thermoplastic replication**
Anders Olsson, Olle Larsson, Johan Holm, Lennart Lundbladh, Ove Öhman and Göran Stemme
Sensors and Actuators A 64 (1998) 63-68.

6 **The first valve-less diffuser gas pump**
Anders Olsson, Göran Stemme and Erik Stemme
1997 IEEE 10th International Workshop on Micro Electro Mechanical Systems (MEMS'97), Jan. 29-31, 1997, Nagoya, Japan.

7 **Numerical and experimental studies of flat-walled diffuser elements for valve-less micropumps**
Anders Olsson, Göran Stemme and Erik Stemme
Submitted for Journal publication

8 **A numerical design study of the valve-less diffuser pump using a lumped-mass model**
Anders Olsson, Göran Stemme and Erik Stemme
Submitted for Journal publication

The contributions of Anders Olsson to the different publications are as follows:

1 All experiments. Part of modeling and writing.
2 Part of fabrication. All experiments. Major part of writing.
3 Part of fabrication. All experiments and modeling. Major part of writing.
4 All design and experiments. Part of fabrication. Major part of writing.
5 All design. Part of fabrication. All experiments. Major part of writing.
6 Part of modeling and writing.
7 All experiments and modeling. Major part of writing.

All modeling. Major part of experiments and writing.

The work has also been presented at the following conferences:

1 **A valve-less planar fluid pump with two pump chambers**
Göran Stemme, Anders Olsson and Erik Stemme
Eurosensor VIII, Sept. 25-28, 1994, Toulouse, France (Invited)

2 **A valve-less planar pump in silicon**
Anders Olsson, Peter Enoksson, Göran Stemme and Erik Stemme
Transducers’95 Eurosensor IX, June 25-29, 1995, Stockholm, Sweden

3 **A valve-less planar pump isotropically etched in silicon**
Anders Olsson, Peter Enoksson, Göran Stemme and Erik Stemme
MME’95, Sept. 3-5, 1995, Copenhagen, Denmark

4 **Valve-less micropumps**
Göran Stemme, Anders Olsson and Erik Stemme
Proceedings of the International Symposium on Microsystems, Intelligent Materials and Robots, Sept. 27-29, 1995, Sendai, Japan (Invited)

5 **Micromachined diffuser/nozzle elements for valve-less pumps**
Anders Olsson, Göran Stemme and Erik Stemme
1996 IEEE 9th International Workshop on Micro Electro Mechanical Systems (MEMS’96), Feb. 10-15, 1996, San Diego, California, USA.

6 **An improved valve-less pump fabricated using deep reactive ion etching**
Anders Olsson, Peter, Enoksson, Göran Stemme and Erik Stemme
1996 IEEE 9th International Workshop on Micro Electro Mechanical Systems (MEMS’96), Feb. 10-15, 1996, San Diego, California, USA.

7 **Microfluidic device research at KTH**
Peter Enoksson, Anders Olsson, Göran Stemme and Erik Stemme
Micro Structure Workshop, March 26-27, 1996, Uppsala, Sweden.

8 **Valve-less diffuser micropumps fabricated using thermoplastic replication**
Anders Olsson, Olle Larsson, Johan Holm, Lennart Lundbladh, Ove Öhman and Göran Stemme
1997 IEEE 10th International Workshop on Micro Electro Mechanical Systems (MEMS’97), Jan. 29-31, 1997, Nagoya, Japan.

9 **Simulation studies of diffuser and nozzle elements for valve-less micropumps**
Anders Olsson, Göran Stemme and Erik Stemme
Transducers’97, June 16-20, 1997, Chicago, Illinois, USA

The contributions of Anders Olsson to the different publications are as follows:

1 All experiments. Part of modeling and writing.
2 Part of fabrication. All experiments. Major part of writing.
3 Part of fabrication. All experiments. Major part of writing.
4 Part of fabrications and experiments.
5 Part of fabrication. All experiments and modeling. Major part of writing.
6 All design and experiments. Part of fabrication. Major part of writing.
7 Part of fabrication, experiments, modeling and writing.
8 All design. Part of fabrication. All experiments. Major part of writing.
9 All modeling. Major part of experiments and writing.

Contents

1 Introduction 3

2 Pumps 4

3 Micromachining technology 5

3.1 Silicon micromachining 5
3.2 Thermoplastic replication 8

4 Actuation principles used in MST 9

4.1 Piezoelectric Excitation 9

5 Micropumps 12

5.1 Peristaltic micropumps 13
5.2 Reciprocating micropumps 13
5.2.1 Reciprocating micropumps with valves *14*
5.2.2 Valve-less reciprocating pumps *16*

6 The valve-less diffuser pump 18

6.1 The diffuser element 18
6.1.1 Diffusers in classical fluid mechanics *19*
6.1.2 Numerical simulations of diffuser elements *23*
6.2 The diffuser pump unit 27
6.2.1 A simple analytic model *28*
6.2.2 An electrical analogy used for designing a gas pump *31*
6.2.3 A lumped-mass model *33*
6.3 Diffuser pump fabrication techniques 36
6.3.1 Conventional technologies *36*
6.3.2 Micromachining *39*
6.4 Results from experiments and simulations 43
6.4.1 Liquid pumping *43*
6.4.2 Gas pumping *49*

7 Summary of appended papers 50

8 Discussion and conclusion 52

9 Outlook 53

10 Acknowledgments 54

11 References 55

1 Introduction

Microengineering is the fabrication of three-dimensional structures in micrometer sizes. Fabricated devices have usually been different types of sensors and actuators on silicon substrates but also other substrates such as quartz can be used. For some applications attempts have been made to use replication of thermoplastics. From having been of interest mainly for scientists at universities and research institutes today micromachining is becoming mature. Ongoing research projects are now often focused on systems and complex components rather than on simple sensors. Manufacturing equipment specially developed for micromachining is now available and the number of commercial products is steadily increasing. Examples of today's volume products are accelerometers, pressure sensors, inkjet printer heads and read/write heads for magnetic hard disk drives [1].

Micro System Technology[1] (MST) is the technology of building systems combining several microcomponents with two or more functions as entire systems. An important part of MST is microfluidic systems. Research on microfluidic devices has its origin about 30 years ago when a gas chromatograph and inkjet printer nozzles were developed [2]. During the subsequent years interest was modest, but during the last decade a dramatic increase in research on microfluidic components has taken place. Microfluidic components fabricated using micromachining technology have the advantage of very small dead volumes and fast response times. Different components have been fabricated including channels, passive and active valves, pumps, flow sensors, filters and mixers [3]. Today microfluidics is a 'hot' research topic. The different components are combined in microliquid-handling systems. Examples of microliquid handling systems are chemical analysis systems, e.g. fluid injection analysis and electrophoresis systems, microdosage systems and systems for counting red blood cells. The continuous demand to reduce sample sizes in analysis systems is an excellent opportunity for MST.

Micromachined pumps are essential in microliquid handling systems. Different micropumps have been developed during the years with different advantages and drawbacks. In this thesis a valve-less pump which uses the flow directing effect of diffuser elements is presented. Several prototypes of different sizes have been fabricated and tested using both conventional fabrication techniques and micromachining technology. The test results have been compared with numerical simulations and classic fluid mechanics in order to understand how the pump works and how to design it to optimize performance. One of the main advantages of the pump is the absence of moving parts, except the pump diaphragms, which reduces the risk of mechanical failure. All the tested pumps show good performance and one of the micromachined versions is very good compared with most of the other presented micropumps. The eight papers in this thesis give full details of the work.

---

[1] Micro System Technology (MST) is the term most used in Europe for what is called Micro Electro Mechanical Systems (MEMS) in USA and Micromachines in Japan.

2 Pumps

The oldest known devices to transfer fluid energy are probably pumps, machines that add energy to fluids [4]. Already 3000 years ago undershoot-bucket waterwheels were used in Asia and Africa and they are still common today. Another early example is Archimedes' screw pump (around 250 BC), still being manufactured to handle solid-liquid mixtures. Generally, pumps can be divided in two basic types, positive displacement pumps and dynamic or momentum-change pumps. Several billions of each type are in use in the world today.

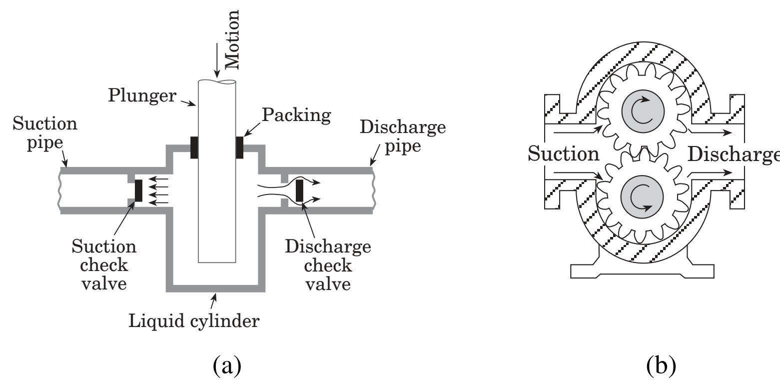

Fig. 2-1. Design of positive displacement pumps: (a) a reciprocating piston or plunger pump and (b) a rotary pump (external gear pump).

In positive-displacement pumps a moving boundary forces the fluid along by volume changes. A cavity opens and the fluid is admitted through an inlet. The cavity is then closed and the fluid is squeezed through an outlet. The classic example is the mammalian heart, but mechanical versions are in wide use which may be classified as rotary pumps and reciprocating pumps, as shown in Fig. 2-1. The reciprocating pumps may further be divided into diaphragm pumps and piston or plunger pumps [4].

All positive-displacement pumps deliver a pulsating or periodic flow as the cavity volume opens, traps, and squeezes the fluid. Their great advantage is the delivery of any fluid regardless of viscosity.

Dynamic pumps simply add momentum to the fluid by means of fast moving blades or vanes or certain special designs. There is no closed volume: the fluid momentum increases while moving through open passages and then converts its high velocity into a pressure increase by exiting into a diffuser section. Dynamic pumps can be classified as rotary pumps and special design pumps, e.g. jet pumps, and for liquid metals electromagnetic pumps.

Dynamic pumps generally provide a higher flow rate and a much steadier discharge than positive-displacement pumps but are ineffective in handling high-viscosity liquids. A positive-displacement pump is appropriate for high-pressure rise and low flow rate, while a dynamic pump provides high flow rate with low-pressure rise.

3 Micromachining technology

Today there exist numerous different processes used for micromachining. Mostly micromechanical devices have been fabricated using silicon micromachining. Another example is the quartz technology used in the watch industry. Attempts have also been made to use other technologies, e.g., thermoplastic replication.

3.1 Silicon micromachining

Historically silicon has been the most commonly used material in MST. The fabrication methods originate from IC manufacturing. Silicon micromachining is usually divided into bulk micromachining and surface micromachining. In bulk micromachining the whole thickness of the silicon wafer is structured while in surface micromachining all the fabrication is done on the surface, as shown in Fig. 3-1.

Single crystalline silicon is characterized by its high Young's modules, about equal to that of steel [5], and low internal losses. It has a diamond cubic crystal structure, shown in Fig. 3-2, which gives it direction dependent anisotropic material characteristics. In the manufacture of silicon wafers for electric devices it is common to orient the wafers along the (100), (110) or (111) plane. The planes are illustrated in Fig. 3-3.

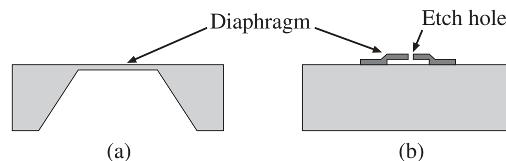

Fig. 3-1. Diaphragms fabricated using (a) bulk micromachining and (b) surface micromachining.

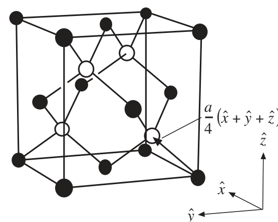

Fig. 3-2. The diamond structure.

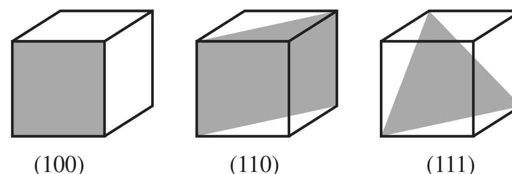

Fig. 3-3. The three crystal planes commonly used for silicon wafer orientation for electronic devices.

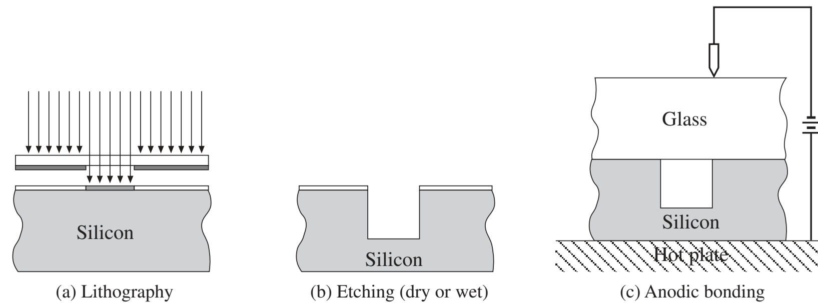

Fig. 3-4. The most important process steps used for valve-less diffuser pumps.

The most important process steps used during this work are summarized below:

Lithography

In the first step a mask is defined on the silicon using a photolithographic process. This mask defines the pattern that should be etched. Different materials can be used as mask materials depending on the following type of process. Silicon dioxide and silicon nitride are probably the most commonly used mask materials, but for dry etching it is also common to use photoresist or a deposited metal, e.g., chromium. The step is illustrated in Fig. 3-4a.

Etching

In the next step the actual etching of the silicon is done. The etching can be done using wet or dry etching. Different etches give different etch profiles as shown in Fig. 3-5.

Wet isotropic etching

Wet isotropic etching ideally is direction independent. How ideal the isotropy is depends on how the etching solution is composed and how the reactants are transported to and from the etching front. A less agitated etching gives flatter bottom. The etching solution is normally based on fluoric (HF), nitric (HNO_3) and acetic acid (CH_3COOH). A typical etch profile is shown in Fig. 3-5a. Silicon dioxide is not useful as mask material since it is etched by the HF. Instead silicon nitride, Si_3N_4, is normally used as the mask material. Isotropic etching is commonly used for chemical polishing of wafers.

Wet anisotropic etching

Wet anisotropic etching is based on the fact that the etch speed in single crystalline silicon is direction dependent. Examples of anisotropic wet etches for silicon are EDP (ethylene diamine, pyrocatechol and water), KOH (potassium hydroxide and water) and TMAH (tetramethyl ammonium hydroxide and water). Typical etching results for KOH are shown in Fig. 3-5b

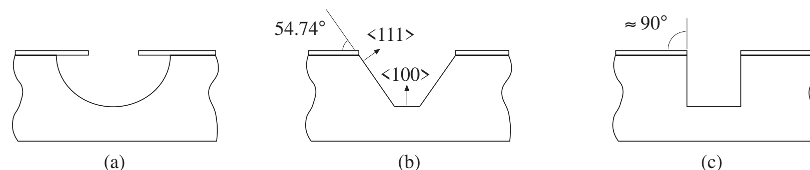

Fig. 3-5. Cross-sectional views of (a) isotropic etch, (b) and (c) anisotropic etch with profiles dependent on the crystal planes and etch method.

where the etching has stopped at the (111) plane. This result is obtained when the mask is oriented parallel to the <110> directions for (100) surface oriented silicon wafers. A result similar to that shown in Fig. 3-5c is obtained if the mask is oriented ± 45° to these directions, i.e. oriented parallel to the <100> direction.

Deep reactive ion etching (DRIE)

Dry etching or reactive plasma etching of silicon is common in micromachining technology. The etching is performed in a chamber at a pressure of 0.5 to 25 Pa. The term reactive plasma describes a discharge in which ionization and fragmentation of gases take place and produce chemically active species. Such plasmas are reactive both in the gas phase and with solid surfaces exposed to them. These interactions are used to form volatile products so that material is removed or etched from surfaces that are not masked by lithographic patterns. The interactions can be divided into two types: physical and chemical. The physical interaction refers to the surface bombardment by energetic ions accelerated across the sheath. Chemical interactions are standard electronic bonding processes that result in the formation or dissociation of chemical species on the surface. Generally the chemical etching is isotropic and the mechanical sputtering is anisotropic. This anisotropy can be enhanced by the choice of gases and other process parameters [6]. Most reactive ion etches are based on chlorine or fluorine processes and common gases are SF_6 and Cl_2.

Today MST is becoming mature. Part of the maturing process is the development of manufacture equipment specially devoted to MST. Recent rapid progress in the development of processes for deep etching of silicon, so called deep reactive ion etch (DRIE), is an example. These processes have both higher etch rates, up to microns per minute, and higher selectivity to the mask material than earlier dry etching processes. Commercial equipment is now available from several sources which can etch straight through a 500 μm thick silicon wafer with almost vertical walls. Aspects ratios higher than 30:1 can be achieved [7]. A cross-section of an etching profile is shown in Fig. 3-5c.

Anodic bonding

Anodic bonding can be used to bond a silicon wafer and a glass wafer together [8]. The glass is normally a sodium glass like Corning 7740. The bonding is carried out at a temperature between 180°C and 500°C when an external voltage in the range 200-1000 V is applied. The bonding process can be monitored by observing the current. When the voltage is applied the current starts with a peak and then decreases. The bond will normally be good when the current has reached about 10-30% of the initial value. Normal bonding time is about 5-10 minutes, but up to half an hour can be necessary. The principle is shown in Fig. 3-4c.

3.2 Thermoplastic replication

Thermoplastic microreplication has interested researchers during recent years. It provides a way of producing microstructure components in high volumes at low cost compared with the more commonly used relatively expensive materials (e.g. single crystalline silicon) and fabrication methods (e.g. silicon etching). Different devices have already been made, e.g. micropumps [9-13]. Microreplication also enables the use of different materials like polymers, metals and ceramics. These factors combined greatly increase the potential use of microstructures in industry.

The principal process steps of thermoplastic microreplication are shown in Fig. 3-6. First a master structure is fabricated using a technique for high precision micromachining. This can be done using deep reactive ion etching of a pattern defined using photolithography. Other possibilities are wet etching or LIGA. From the master a negative mold insert is made by electroplating. This mold is then used in a micromolding process where a large number of plastic replicas are fabricated. Examples of techniques are injection molding and hot embossing.

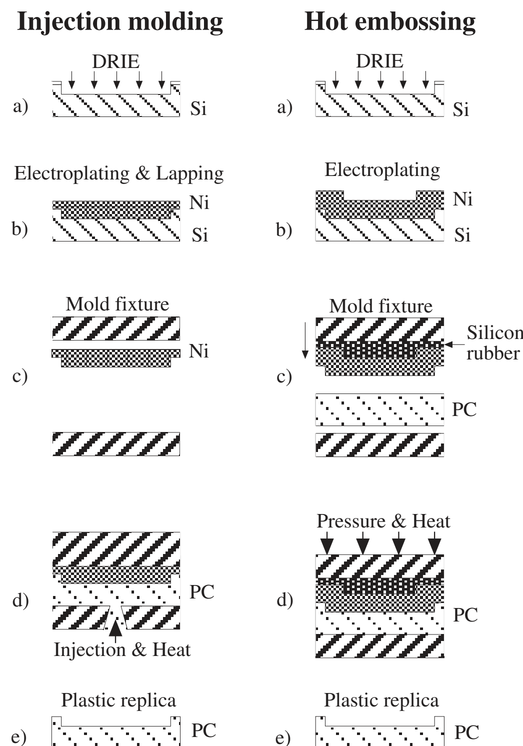

Fig. 3-6. The main process steps used in two different thermoplastic replication methods.

4 Actuation principles used in MST

Today actuators are an important part of MST. Consequently a lot of research is devoted to actuators. Actuators are needed to transfer input energy, e.g. electric or thermal energy, into work output, e.g. motion, heat or light (see Fig. 4-1). Many resonant sensors, e.g. gyros, require actuators to drive them. Actuators can be used to build in self-testing in sensors that previously only had detection capabilities. Microsystems that require mechanical output need actuators. Examples of such systems are micromirrors used to scan laser beams or to switch them from one fiber to another. In microfluidic system and microanalysis systems actuators are needed for pumps and valves. They can also be used for switches, relays, etc., in microelectromechanical devices for wireless communications.

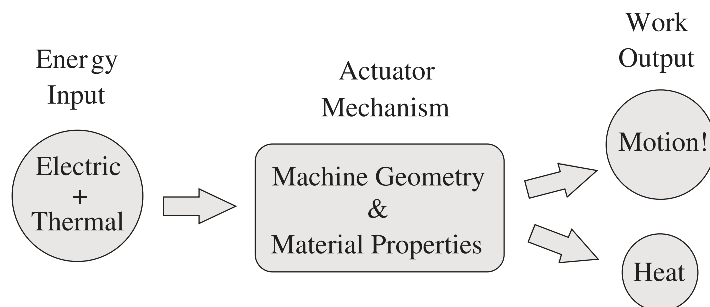

Fig. 4-1. A schematic figure of the transfer of input energy to output work in an actuator [14].

Many different solutions for actuation of micromechanical devices have been proposed. Piezoelectric actuation is probably the most commonly used method for micropumps but other methods have also been used, e.g. electrostatic, pneumatic and thermopneumatic excitation. During this project the focus was on the pump principle rather than the actuation principle. Piezoelectric actuation was chosen because it can easily be applied to the individual pumps after the micromachining process.

4.1 Piezoelectric Excitation

The piezoelectric force has been widely used for micromechanical devices. The effect was discovered by Jacques and Pierre Curie in 1880. They discovered that if special crystals were subject to mechanical tension, they became electrically polarized and the polarization was proportional to the extension. They also discovered that the opposite was true; If an electrical field was applied across the material it deformed. This is known as the inverse piezoelectric

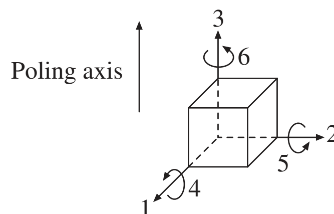

Fig. 4-2. The notation of the axes for piezoelectric ceramics [15]

effect. Piezoelectricity involves the interaction between the electrical and mechanical behavior of the medium. To the first order this is described as [15]

$$\boldsymbol{S} = \boldsymbol{s}^E \boldsymbol{T} + \boldsymbol{dE} \tag{4-1}$$

where $\boldsymbol{S}$ is the strain, $\boldsymbol{s}^E$ is the compliance tensor under conditions of constant electric field, $\boldsymbol{T}$ is the stress, $\boldsymbol{d}$ is the piezoelectric charge constant tensor and $\boldsymbol{E}$ is the electric field. The deformation of a piezoelectric crystal is illustrated in Fig. 4-3. In the absence of mechanical loads Eq. (4-1) gives

$$\Delta l = d_{33} \cdot U = d_{33} \cdot \frac{U}{l} \cdot l = d_{33} \cdot E \cdot l \tag{4-2}$$

and

$$\Delta a = d_{31} \cdot U = d_{31} \cdot \frac{U}{l} \cdot a = d_{31} \cdot E \cdot a \tag{4-3}$$

where Δl is elongation along the poling axis, l is the device length along the poling axis, U is the electrical voltage, Δa is elongation perpendicular the poling axis and a is the device length perpendicular to the poling axis. Normally $d_{33} > 0$ and $d_{31} < 0$.

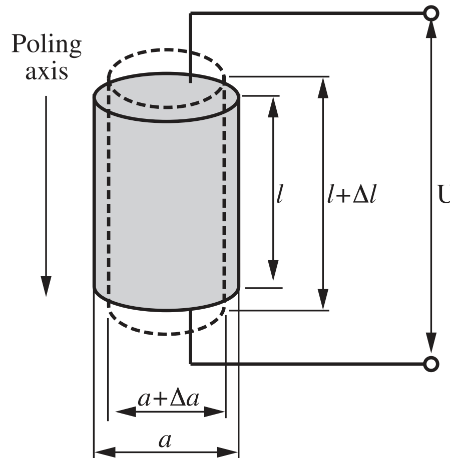

Fig. 4-3. The deformation of a piezoelectric device when subject to an electrical voltage [14].

Examples of piezoelectric materials are quartz, $LiTaO_3$, PZT and ZnO. Non-piezoelectric materials, e.g. silicon, can be exited by depositing a thin film of a piezoelectric material, e.g. PZT or ZnO. Another solution is to mount a piezoelectric disk on the non-piezoelectric material. This eliminates the problem of making the film thick enough that high voltages can be applied without dielectric breakdown (sparks/short circuits across the film). The piezoelectric effect can be used to bend a diaphragm, e.g., in a pump. The principle is illustrated in Fig. 4-4 where a piezoelectric disk is glued to a diaphragm. When a voltage is applied across the piezoelectric disc it deforms and forces the diaphragm to bend.

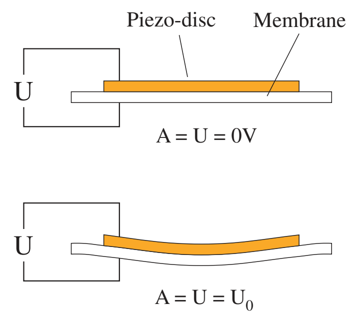

Fig. 4-4. The bending of a bimorf consisting of a piezoelectric disc glued on a membrane. This can be used for diaphragm pumps.

5 Micropumps

Research on micropumps was initiated in 1980 and numerous different pumps have since been developed [2]. They can be manufactured in different materials, but mostly silicon and glass have been used as bulk materials. During the last years plastic has been shown to be a competitive alternative. Different pump principles are conceivable. They can generally be classified into two groups: mechanical and non-mechanical (without moving parts) [16]. At least three kinds of mechanical micropumps have been developed: peristaltic [17], reciprocating [18-20] and rotary [21] pumps. In Table 5-1 the performances of some mechanical micropumps are summarized. The pumps that have attracted most attention are reciprocating diaphragm pumps, mainly because of the broad range of fluids which can be pumped and because the pumps are readily realized using silicon micromechanics. In non-mechanical micropumps the electrodynamic effect, electroosmotic phenomena and ultrasonic effect are used among others [16].

Table 5-1. Characteristics of mechanical micropumps

Author year [reference]	Pump principle	Actuation mechanism	Pump frequency [Hz]	Volume flow** [μl/min]	Pressure head** [kPa]	Size [mm]	Comment
Ahn 1995 [21]	Jet-type rotary	electro-magnetic	83	24	-*	2×2×0.16	Liquid: regular insulin
Smits 1990 [17]	Peristaltic	piezoelectric, disc type	15	100	6	-*	
Mizoguchi 1992 [22]	—"—	thermal (laser)	3	5	0.3	-*	
van Lintel et al 1988 [18]	Reciprocating, check-valves	piezoelectric, disc type	3	8	10	Ø50×2	
van de Pol et al 1990 [23]	—"—	thermo-pneumatic	1	34	5	13×45×2	
Shoji et al 1990 [24]	—"—	piezoelectric, stack type	40	40	15	20×20×1	
Zengerle et al 1992 [25]	—"—	electrostatic	25	70	2.5	7×7×2	
Lammerink et al 1993 [26]	—"—	thermo-pneumatic	5	60	4	13×45×2	
Stemme & Stemme 1993 [20]	Reciprocating, valve-less diffuser	piezoelectric, disc type	300	3000	25	19×5	
Olsson et al 1994	—"—	piezoelectric, disc type	560	16000	17	36×36×1	Brass
Gerlach et al 1994 [27-29]	Reciprocating, valve-less nozzle	piezoelectric, disc type	8000	480	3.3	-*	
Olsson et al 1995	Reciprocating, valve-less diffuser	piezoelectric, disc type	1300	225	17	15×18×1	Isotropically etched
Zengerle et al 1995 [19]	Reciprocating, check-valves	electrostatic	0-1000	350	31	7×7×2	Bi-directional
Zengerle et al 1996 [30]	Reciprocating, active valve	piezoelectric	60	1600	17	7.3×7.3*** and 5.3×5.3***	Bi-directional
Olsson et al 1996	Reciprocating, valve-less diffuser	piezoelectric, disc type	3000-4000	2300	74	15×17×1	DRIE
Kämper et al 1998 [13]	Reciprocating, check-valves	piezoelectric, disc type	50-70	400	210	12×12×3.5	Self-priming Plastic
Linnemann et al 1998 [31]	Reciprocating, check-valves	piezoelectric, disc type	220	1400	1000	7×7×1.1 and 15×7	Self-priming

* Information not found   **Pump liquid is water   ***Size of the diaphragm

5.1 Peristaltic micropumps

Two types of peristaltic micropumps have been reported using piezoelectric disks [17] and thermopneumatic actuators [22]. The peristaltic micropump using piezoelectric disks was the first developed micropump. The pump comprising three active valves in line is illustrated in Fig. 5-1. Each valve consists of a chamber with inlet and outlet each covered by a flexible membrane. By deflecting the membrane, which was made of two piezoelectric discs, an underpressure was generated. The pump was able to pump 100 μl/min without a pressure difference between inlet and outlet and was able to reach a maximum pump pressure of 60 cm H_2O.

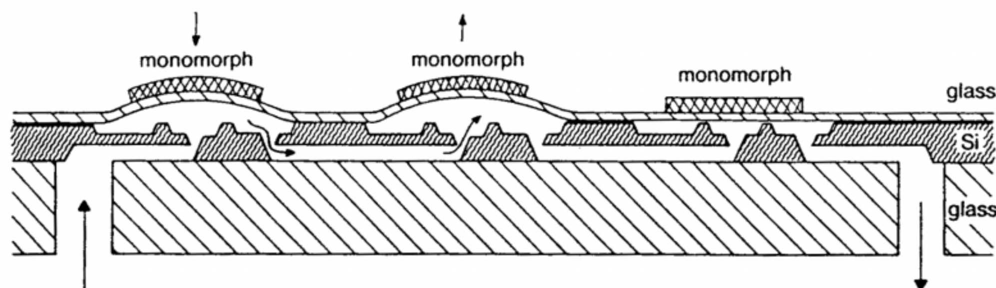

Fig. 5-1. The first micropump. The pump is piezoelectrically actuated and includes three valves working peristaltically [17].

5.2 Reciprocating micropumps

Micropumps of the reciprocating type consist of a pressure chamber having a flexible diaphragm driven by an actuator and flow directing elements. The flow directing elements and the actuator play important roles in the flow rate and the maximum pressure. Many types of actuators like piezoelectric, pneumatic, electrostatic and thermopneumatic have been used. The maximum output pressure of the micropumps is dependent on the available force of the actuators used.

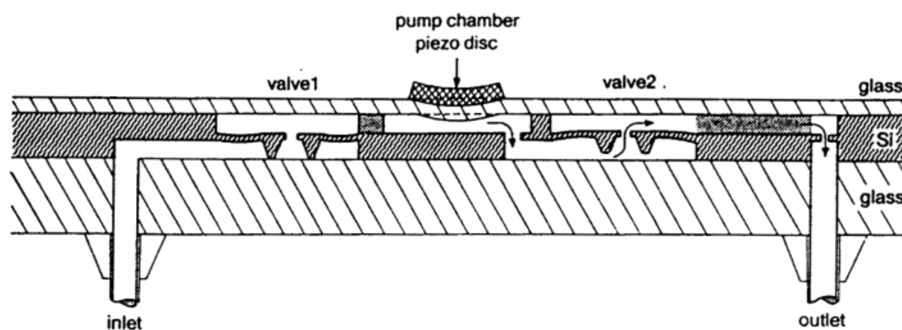

Fig. 5-2. A piezoelectric two-valve pump [18].

5.2.1 Reciprocating micropumps with valves

Based on the first peristaltic pump [17] two improved pumps of the reciprocating displacement type were developed [18]. These pumps had one or two pump chambers and a thin glass pump membrane actuated by a piezoelectric disc. They used passive silicon check valves to direct the flow, see Fig. 5-2. Based on the same principle another pump, shown in Fig. 5-3, was developed which used electro-thermopneumatic actuation instead of piezoelectric actuation [23].

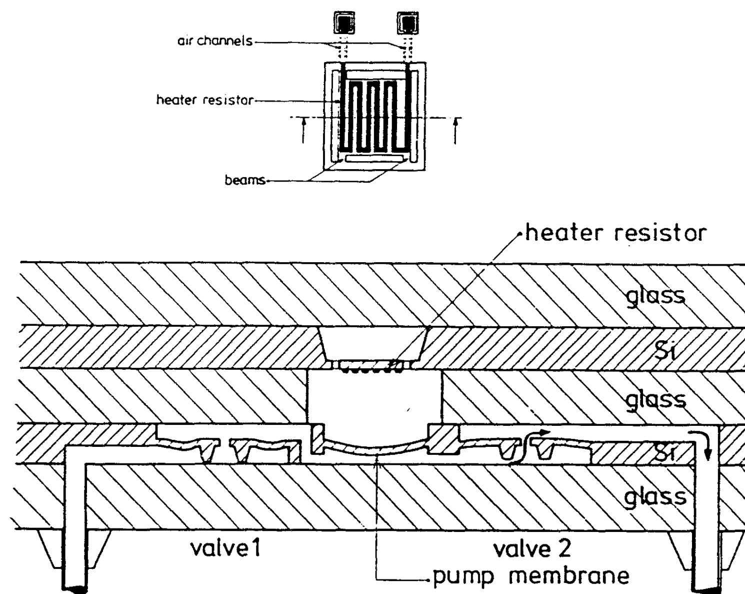

Fig. 5-3. A thermopneumatic micropump [23].

Later several different diaphragm pumps with different actuation principles have been developed. One of the most interesting used an electrostatic actuation principle [25] and was further developed into the bi-directional pump [19], illustrated in Fig. 5-4. This pump works in the forward direction for low frequencies (0.1-800 Hz) and in the reverse direction for higher frequencies (2-6 kHz).

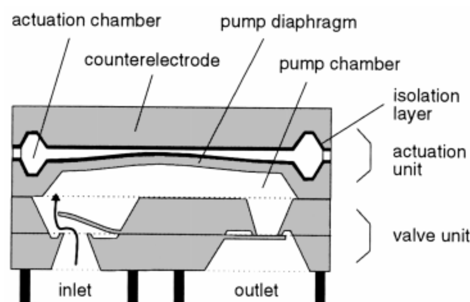

Fig. 5-4. A bi-directional silicon micropump with passive check valves [19].

A silicon pump illustrated in Fig. 5-5 based on the same principle but with piezoelectric actuation has recently been presented [31]. The pump can pump both liquids and gases, shows very good performance and is able to fill itself. This self-filling capability has been achieved by minimizing the dead volumes of the pump in order to maximize the compression ratio in the pump chamber during a pump cycle.

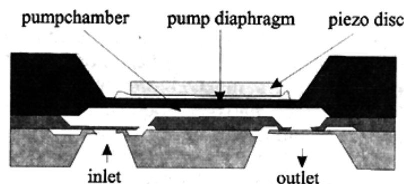

Fig. 5-5. A self-priming and bubble-tolerant piezoelectric silicon micropump for liquids and gases [31].

At the same time, another pump illustrated in Fig. 5-6 was presented that also uses piezoelectric actuation [13]. This pump is also self-priming and works with both liquids and gases. It is interesting because it is fabricated in plastic at low cost and it shows very good performance.

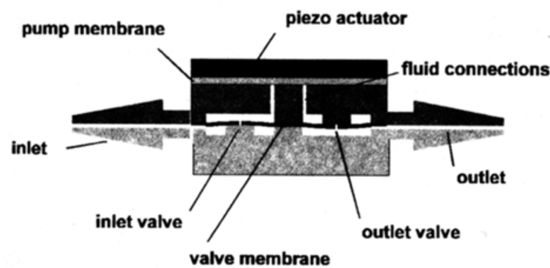

Fig. 5-6 A self-filling membrane micropump in thermoplastic [13].

A micropump based on a totally different pump mechanism is shown in Fig. 5-7 [30]. The pump diaphragm acts as an active valve and two new pump mechanisms called "the Elastic Buffer mechanism" and "the Variable Gap mechanism" are used. The direction of the fluid transport can be switched by varying the driving frequency. The pump was shown to work for both liquid and gas and was the first liquid self-priming micropump.

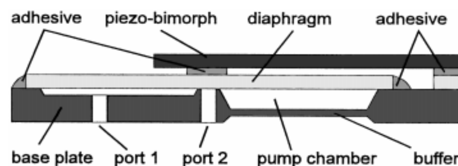

Fig. 5-7. The bi-directional micropump with self-blocking effect (VAMP) [30].

5.2.2 Valve-less reciprocating pumps

Valve-less reciprocating pumps have flow channels at the inlet and the outlet that are designed to have different flow resistances in the forward and the reverse directions. This eliminates wear and fatigue in the check-valves and reduces the risk of valve clogging. The idea to use such channels in pumps was mentioned in 1989 [32] and a finite element analysis of micromachined nozzles used as such channels was presented in 1990 [33].

The first valve-less reciprocating pump was the valve-less diffuser pump presented in 1993 [20, 34] and illustrated in Fig. 5-8. In the diffuser pump diffuser elements are used as the flow directing elements. The opening angles of the diffusers are small, normally less than 20°, and the diffuser direction is the positive flow direction.

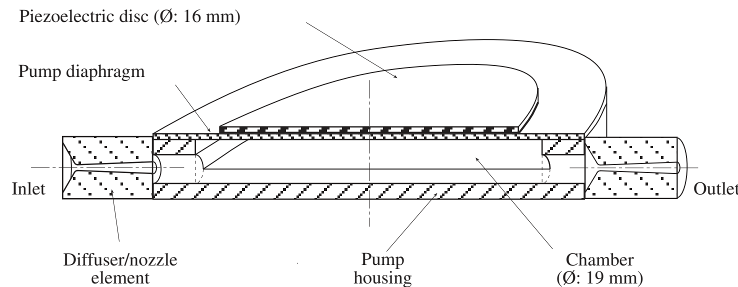

Fig. 5-8. Cross-sectional view of the single-chamber metal (brass) pump consisting of a circular housing with an oscillating top diaphragm and two conical diffuser elements [20].

In 1994 the valve-less pump shown in Fig. 5-9 using nozzles with an opening angle of 70.5° was presented [28, 29]. The pump is fabricated in silicon using anisotropic wet etching. The sharp inlet and outlet together with the large opening angle defined by the <111>-planes in the silicon makes the converging wall direction the forward direction and the diverging wall direction the reverse direction. Consequently, the pump works in the opposite direction compared with the earlier presented valve-less diffuser pump, which has its forward direction in the diverging wall direction.

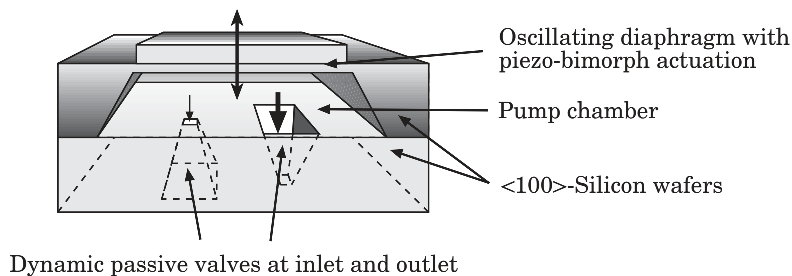

Fig. 5-9. The valve-less micropump with dynamic passive-valves [28].

A third type of valve-less micropump was proposed in 1995 [35]. This pump uses the valvular conduit [36] shown in Fig. 5-10 as flow directing element. Valvular conduits have been fabricated using micromachining technology and shows a direction dependent flow behavior, but no data for pump performance was found [35].

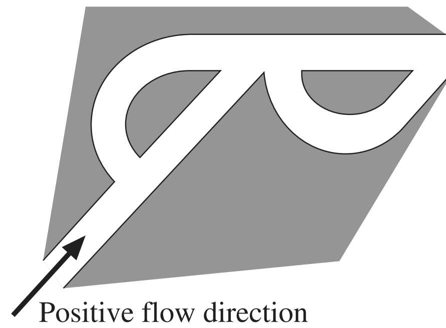

Fig. 5-10. The geometry of a valvular conduit. The geometry is designed to give a lower flow resistance in the positive flow direction than in the opposite, the negative, flow direction [35, 36].

6 The valve-less diffuser pump

The first valve-less diffuser pump was presented in 1993 [20, 34]. It uses diffuser elements as flow directing elements. Wear and fatigue in the valves are therefore eliminated since the diffuser elements have no moving parts and the risk of valve clogging is also reduced. The idea of using flow channels with flow direction dependent flow resistance as illustrated in Fig. 6-1 was mentioned in 1989 [32]. A finite element analysis of micromachined nozzles used as such channels was presented in 1990 [33].

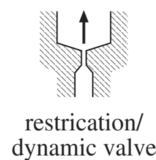

Fig. 6-1. The restriction/dynamic valve proposed in [32].

The diffuser pump is a positive displacement pump in the sense that it has a moving boundary that forces the fluid along by volume changes. As other positive displacement pumps it delivers a periodic flow. The pump principle has been shown to work for different liquids and for air.

6.1 The diffuser element

The diffuser, a flow channel with gradually expanding cross-section, is the key element in the valve-less diffuser pump. Used in the opposite direction with converging cross-section it is called a nozzle. Diffusers usually have circular or rectangular cross-sections as illustrated in Fig. 6-2. They are called conical and flat-walled diffusers, respectively. Both diffusers and nozzles are common devices in macroscopic internal flow systems.

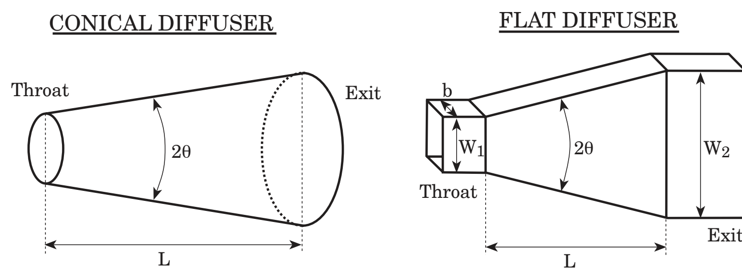

Fig. 6-2. Flat-walled and conical diffusers.

6.1.1 Diffusers in classical fluid mechanics

The function of the diffuser is to transform kinetic energy, i.e. velocity, to potential energy, i.e. pressure. The type of flow in a diffuser can be exemplified by a 'stability map', such as shown in Fig. 6-3 [4]. The map shows that depending on the diffuser geometry, the diffuser operates in four different regions. In the *no stall* region the flow is steady viscous without separation at the diffuser walls and moderately good performance. In the *transitory steady stall* region the flow is unsteady. The minimum pressure loss occurs in this region. In the *bistable steady region* a steady bistable stall can flip-flop from one part of the diffuser wall to another and performance is poor. In the *jet flow* region the flow separates almost completely from the diffuser walls and passes through the diffuser at nearly constant cross-sectional area making performance extremely poor.

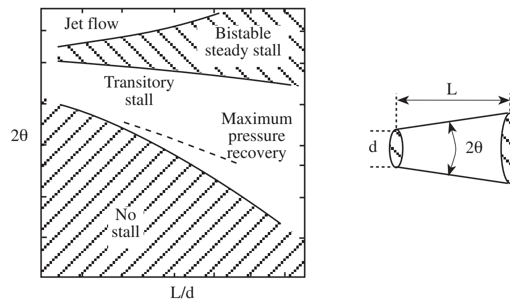

Fig. 6-3. A stability map of a diffuser. A stability map can be used to design a diffuser geometry with minimal pressure loss coefficient. This is shown as a dashed line in the transitory stall region [4].

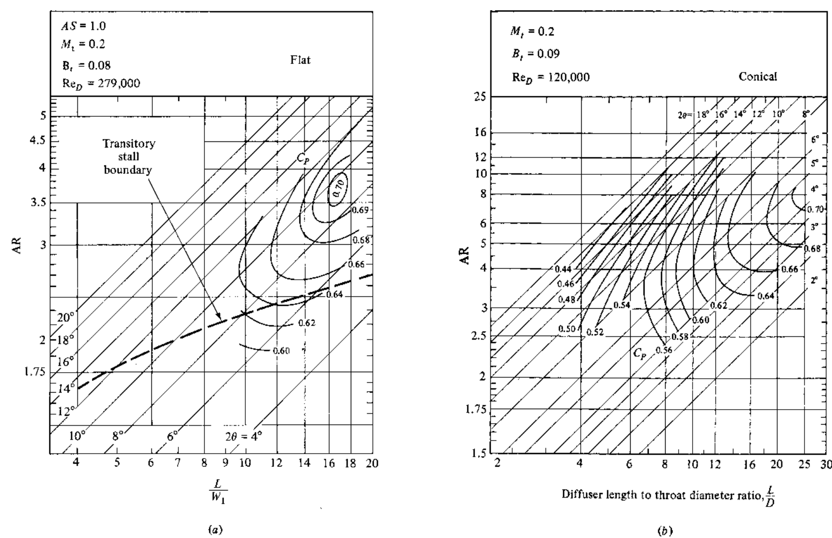

Fig. 6-4. Typical performance maps for a flat-wall diffuser and conical diffusers at similar operating conditions: (a) flat-wall and (b) conical [37].

Typical performance maps for diffusers are shown in Fig. 6-4 [37]. The higher the C_P value, the better is the diffuser performance. In general, the two main types of diffusers, conical and flat-walled, have approximately the same diffuser capacity. However, the best performance for conical diffusers is achieved at a length that is 10 to 80 percent longer than for the best flat-walled design [4]. The choice of diffuser type depends mainly on the fabrication process, but flat-walled diffusers are preferred since they give a more compact design.

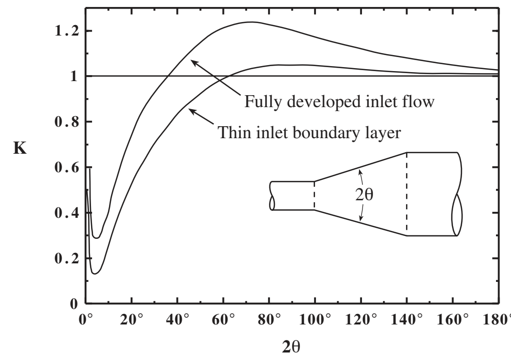

Fig. 6-5. Flow losses in a gradual conical expansion region [4, 37].

In Fig. 6-5 the dependence of the losses on diffuser angle is shown for diffusers with macroscopic, turbulent flow[4, 37]. The loss coefficient is related to the C_P value by the relation

$$K = 1 - \left(\frac{A_{in}}{A_{out}}\right)^2 - C_P \tag{6-1}$$

where A_{in} and A_{out} are the inlet and outlet cross sectional areas, respectively. For small angles the losses in the diffuser are small and the minimum losses occur for a cone angle 2θ equal to about 5°. For cone angles larger than 40° to 60° the loss is higher than for a sudden expansion. For these large angles, the gradual expansion does not raise the static pressure further and there is no diffuser effect. This unexpected effect is due to gross flow separation in a wide-angle diffuser [4]. The effect is highly dependent on the inlet boundary conditions.

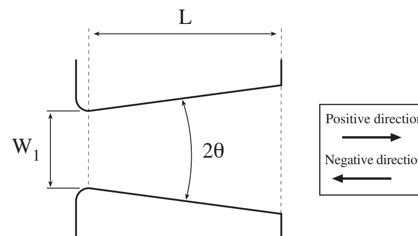

Fig. 6-6. Diffuser element geometry.

A diffuser element is a diffuser with inlet and outlet as illustrated in Fig. 6-6. In order to achieve the best pump performance the diffuser element has to be designed for highest possible flow directing capability. To estimate the possible flow directing capability of a diffuser element available information for macroscopic internal flow systems with circular cross-section was used. The pressure drop in an internal flow system is usually given as the loss coefficient, K, which is related to the pressure drop, Δp, by

$$\Delta p = K \cdot \frac{1}{2} \rho \bar{u}^2_{upstream} \tag{6-2}$$

where ρ is the fluid density and $\bar{u}_{upstream}$ is the mean velocity upstream. For the complete diffuser element it is more practical to relate the pressure drop to the velocity in the narrowest cross-section, the throat, as

$$\Delta p = \xi \cdot \frac{1}{2} \rho \bar{u}^2_{throat} \tag{6-3}$$

where ξ is the pressure loss coefficient and $\bar{u}_{throat}$ is the mean velocity in the throat. The relation between ξ and K is then the simple area relation

$$\xi = K \cdot \left(\frac{A_{throat}}{A_{upstream}} \right)^2 . \tag{6-4}$$

With this definition the diffuser element efficiency ratio η can be defined as

$$\eta = \frac{\xi_{negative}}{\xi_{positive}} . \tag{6-5}$$

To optimize the efficiency of the diffuser element the ratio η should be maximized. To achieve this the entrance region of the diffuser in Fig. 6-6 should be rounded [4]. As shown above the part with expanding cross-section shows best performance with an opening angle 2θ of about 5°. The outlet should be sharp. Using pressure loss coefficients for macroscopic flows this gives a maximum diffuser element efficiency of $\eta = 3.6$ [4]. The calculations are shown in Fig. 6-7.

The same type of empirical analysis as made for the diffuser element can be made for a wide angle conical channel with sharp inlet, a nozzle element. The used dimensions together with the resulting pressure loss coefficients are summarized in Fig. 6-7. The analyze shows that the converging-wall direction is the positive direction. That is the opposite direction compared with the diffuser element. The resulting efficiency ratio for the nozzle element is $\eta \approx 1.45$. For an element with a rounded inlet it is reduced to $\eta \approx 1.10$.

This is described in detail in papers 3 and 7.

	$k = \frac{A_{throat}}{A_{upstream}}$	Diverging-wall Direction	Converging-wall Direction	$\eta = \frac{\xi_{negative}}{\xi_{positive}}$
Diffuser Element	$\left(\frac{0.23}{0.6}\right)^2 \approx 0.15$	$K_{in}=0.05 \Rightarrow \xi_{in}=0.05$ $C_P=0.77 \Rightarrow K_{diverging}=1-k^2-0.77=0.21 \Rightarrow \xi_{diverging}=0.21$ $K_{out}=1 \Rightarrow \xi_{out}=1 \cdot k^2 \approx 0.02$ $\xi_{positive}=\xi_{in}+\xi_{diverging}+\xi_{out} \approx 0.28$	$K_{in}=0.4 \Rightarrow \xi_{in}=0.4 \cdot k^2 \approx 0.009$ $K_{converging}=0.03 \Rightarrow \xi_{converging}=0.03 \cdot k^2 \approx 0.0006$ $K_{out}=1 \Rightarrow \xi_{out}=1$ $\xi_{negative}=\xi_{in}+\xi_{converging}+\xi_{out} \approx 1.009$	$\frac{1.009}{0.28} \approx 3.60$
		Sharp inlet: $K_{in}=0.4 \Rightarrow \xi_{in}=0.4 \Rightarrow \xi_{positive}=0.63$		$\frac{1.009}{0.63} \approx 1.60$
Nozzle Element	$\left(\frac{0.241}{0.76}\right)^2 \approx 0.10$	$K_{in}=0.4 \Rightarrow \xi_{in}=0.4$ $K_{diverging}=1.05 \Rightarrow \xi_{diverging}=1.05$ $K_{out}=1 \Rightarrow \xi_{out}=1 \cdot k^2 \approx 0.01$ $\xi_{negative}=\xi_{in}+\xi_{diverging}+\xi_{out} \approx 1.46$	$K_{in}=0.4 \Rightarrow \xi_{in}=0.4 \cdot k^2 \approx 0.004$ $K_{converging}=0.07 \Rightarrow \xi_{converging}= =0.07 \cdot k^2 \approx \approx 0.0007$ $K_{out}=1 \Rightarrow \xi_{out}=1$ $\xi_{positive}=\xi_{in}+\xi_{converging}+\xi_{out} \approx 1.005$	$\frac{1.46}{1.005} \approx 1.45$
		Rounded inlet: $K_{in}=0.05 \Rightarrow \xi_{in}=0.05 \Rightarrow \xi_{negative}=1.11$		$\frac{1.11}{1.005} \approx 1.10$

Fig. 6-7. The different loss coefficients [4], K, and pressure loss coefficients, ξ, for a small angle conical diffuser element with the throat diameter $d_{\min} = 0.23$ mm and the outlet diameter $d_{\max} = 0.6$ mm [20] and a wide angle conical nozzle element with $d_{\min} = 0.241$ mm and $d_{\max} = 0.76$ mm (compare [28, 29, 38]).

6.1.2 Numerical simulations of diffuser elements

Analytic expressions describing physical phenomena are normally useful and make it possible to do studies of the effects of different parameters on the solution. The problem is that in many cases no explicit analytic expression can be found. This is especially true for fluid mechanics. Then numerical methods have to be used. Today there exist numerous different commercial software packages that can be used for numerical simulations.

Computational Fluid Dynamics (CFD) is the term commonly used for numerical simulations of fluid flows. CFD-software can be based on different methods, e.g. finite elements or finite volumes. Usually the structure is divided into substructures and symmetries are used to reduce the model size in order to minimize the computer time. It is also common to use two-dimensional models. Examples of the use of CFD-software for micromachined devices are found in e.g. [33, 39-41].

There are two basic ways to make a continuous equilibrium problem discrete. One way is to choose a finite number of points and to replace derivatives by differences. The other way is to choose a finite number of functions and to approximate the exact solution by a combination of those trial functions. If the functions are chosen as piecewise polynomials, then the pieces can be chosen to fit the geometry of the problem and the computer can generate the polynomials. This is the idea behind the finite element method [42].

6.1.2.1 The Finite Element Method

The finite element method is commonly used for analyzing structures and continua. It was originally developed as a method for stress analysis, but today it is also used to solve problems in electric and magnetic fields, fluid flow, heat transfer, lubrication and many other fields [43]. The finite element method models a structure as an assemblage of small parts (elements). Each element has a simple geometry and therefor is easier to analyze than the actual structure. A complicated solution is approximated by a model that consists of piecewise continuous simple solutions and the elements are called ”finite” to distinguish them from differential elements used in calculus. The type of element used in the model and the number of elements are important for the accuracy of the solution.

The finite element method can be very versatile. It can be applied to various physical problems where the analyzed body can have arbitrary shape, loads and support conditions. Another attractive feature is the close physical resemblance between the actual structure and its finite element model. A disadvantage of the finite element method is that a specific numerical solution is found for a specific problem. No closed form solution permits analytical study of the effects of changing the different parameters. It is also necessary to have experience and good engineering judgment in order to define a good model.

6.1.2.2 CFD-simulations using ANSYS/FLOTRAN

ANSYS/FLOTRAN is a CFD program which is a part of the commercial software package ANSYS. It is based on the finite element method and offers different types of analyses, e.g. laminar or turbulent flow and compressible or incompressible flow. Laminar flow analysis should be used typically for highly viscous, slow-moving flow where the velocity field is usually very ordered. Turbulent flow analysis is used when the velocity is high enough and the viscosity low enough to cause turbulent fluctuations. The fluid is assumed Newtonian, it is assumed to be only one phase, the problem domain is assumed not to change and the user must

determine if the problem is laminar or turbulent and if it is incompressible or compressible. The fluid flow problem is defined by laws of conservation of mass, momentum[2] and energy [44]. For incompressible flow with constant properties they reduces to [4]

Conservation of mass: $$\nabla \cdot \boldsymbol{V} = 0 \quad (6\text{-}6)$$

Conservation of momentum: $$\rho \frac{D\boldsymbol{V}}{Dt} = \rho \boldsymbol{g} - \nabla p + \mu \nabla^2 \boldsymbol{V} \quad (6\text{-}7)$$

Conservation of energy: $$\rho c_v \frac{DT}{Dt} = \kappa \nabla^2 T + \Phi \quad (6\text{-}8)$$

where $\boldsymbol{V}$ is the velocity vector, ρ is the density, D/Dt is the substantial derivative, $\boldsymbol{g}$ is the gravity force vector, μ is the coefficient of viscosity, c_v is the specific heat at constant volume, T is the temperature, K is the coefficient of thermal conductivity of the fluid and Φ is the viscous dissipation function.

The turbulence model used in ANSYS/FLOTRAN is the k-ε-model. It is a two equation turbulence model which accounts for the effect of the turbulent viscosity fluctuations of the mean flow. The effective viscosity, μ_ε, is defined as [45]

$$\mu_\varepsilon = \mu + \mu_t \quad (6\text{-}9)$$

where μ is the laminar viscosity and μ_t is the turbulent viscosity. The latter is calculated of the program. The manual for FLOTRAN gives the advice that the mean value of μ_t should be at least five times higher than μ to use the turbulent flow model. User defined turbulence models were not possible to implement in the version of ANSYS/FLOTRAN (ANSYS/Multiphysics 5.3) used here.

ANSYS/FLOTRAN was used to simulate the flow behavior for different diffuser elements using both two- and three-dimensional models. All simulations were done using water as liquid thereby limiting the problem to incompressible flow. To determine if the flow is laminar or turbulent is more difficult. The normal way is to evaluate the Reynolds number and compare it to the transitional number. The Reynolds number, *Re*, for a diffuser is usually defined as

$$Re = \frac{d \cdot \overline{u}}{\nu} \quad (6\text{-}10)$$

where d is the width of the diffuser throat, $\overline{u}$ is the mean velocity in the throat and ν is the kinematic viscosity of the liquid. The transition number for macroscopic flow in pipes with smooth walls is approximately 2300 [46]. This value may be different for microfluidic flow due to the small dimensions and may for the flat-walled diffuser elements in paper 1, 4 and 7 be estimated to approximately 400 [2]. The transition to turbulence is also effected of the smoothness of the walls and the pressure gradient [46]. Thus simulations were done for both laminar and turbulent flow. The simulations are compared with experimental results in section 6.4.1.1.

---

[2] The equation for conservation of momentum is normally turned into the Navier-Stokes equation.

Typical laminar flow patterns for a diffuser element with length 1.093 mm, throat width 80 μm and opening angle 9.8° is shown in Fig. 6-8. In the diverging-wall direction the laminar solution shows a small asymmetry at the outlet that not is seen for the turbulent solution. The pressure recovery seen between the throat and the exit in Fig. 6-9 is important for the function of the element. The diverging-wall direction is the positive flow direction.

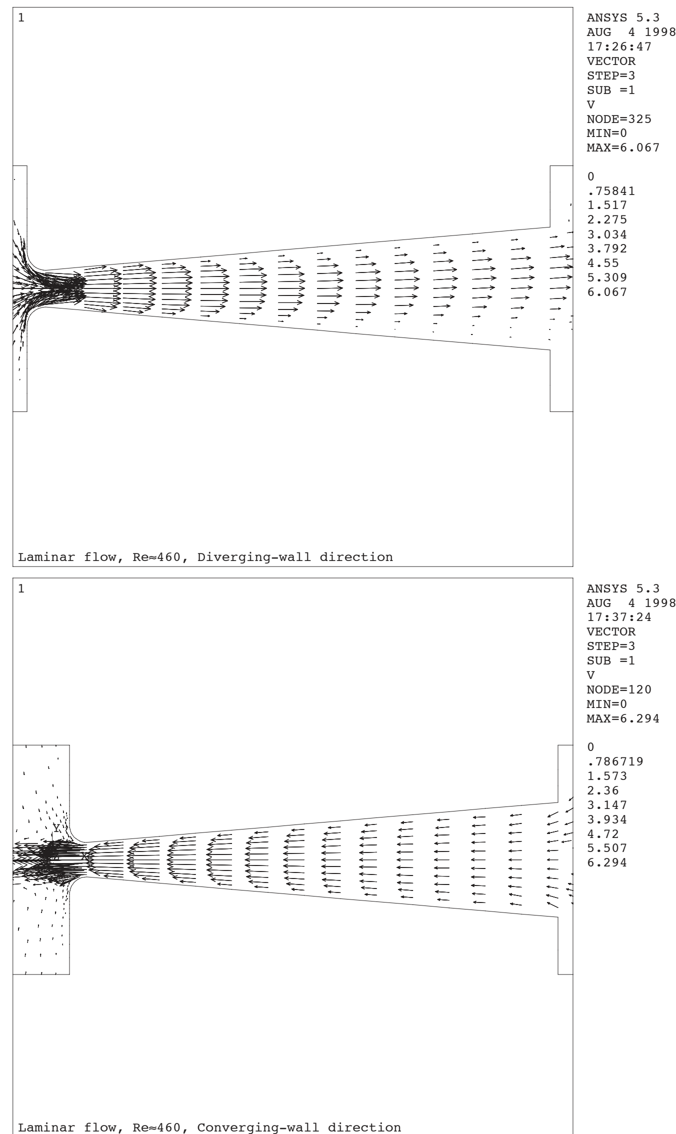

Fig. 6-8. Flow patterns simulated for a 2-dimensional model of a diffuser element of length 1.093 mm, opening angle 9.8° and smallest width 80μm. The laminar flow model was used and the number of elements is fewer than normally used to make the arrows clearer.

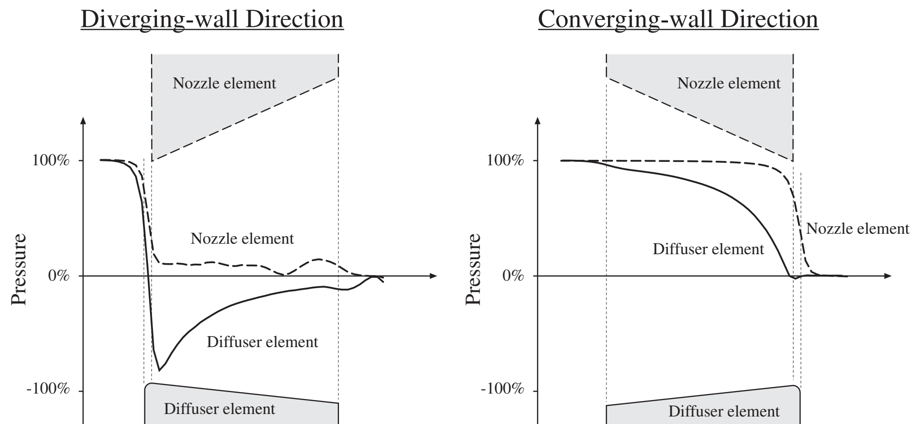

Fig. 6-9. Pressure distribution along the symmetry axis.

This can be compared an element with a diffuser opening angle of 70 and where both the inlet and the outlet are sharp (compare the nozzle pump in [28, 29, 38]). Typical flow pattern is shown in Fig. 6-10. For this large opening angle the losses are in fact higher than for a sudden expansion and thus the flow directing principle is not based on diffuser pressure recovery. Instead, it relies on the ”vena-contracta” effect. The pressure distribution along the center axis shows (Fig. 6-9) that there is almost no pressure recovery in the diverging-wall part of the nozzle element.

This is described in detail in paper 7.

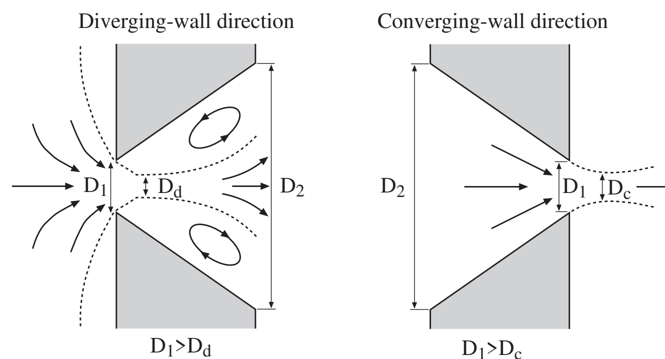

Fig. 6-10. The "vena-contracta" effect for wide angle flow channels used in the valve-less nozzle pump.

6.2 The diffuser pump unit

The basic element in the diffuser pump unit consists of two diffuser elements connected to a fluid cavity volume with an oscillating diaphragm as shown schematically in Fig. 6-11. The pump operation is based on the flow directing properties of the two diffuser elements. With correctly designed diffuser elements more fluid flows through the inlet element than through the outlet element during the supply mode. During the pump mode more fluid flows through the outlet element than through the inlet element. This results in a net flow from the inlet side to the outlet side of the pump unit.

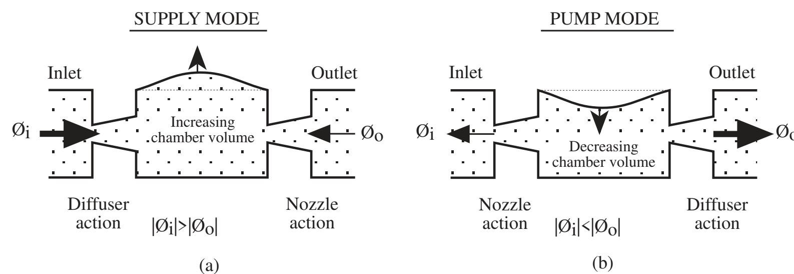

Fig. 6-11. Operation of the diffuser-based pump (single-chamber and single-diaphragm): (a) supply mode; (b) pump mode.

Like all positive-displacement pumps the diffuser pump delivers a pulsating or periodic flow. To reduce this and improve the pump performance two pump cavities can be connected in parallel working in anti-phase, as illustrated in Fig. 6-12. Theoretically, this will also double the pump flow compared to a single chamber pump.

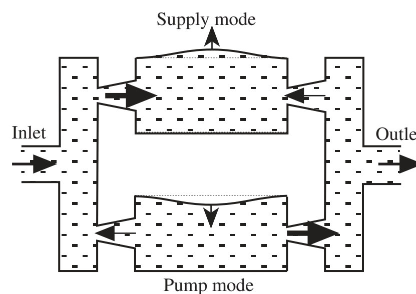

Fig. 6-12. Push-pull anti-phase operation of the parallel arrangement of a double-chamber diffuser pump.

6.2.1 A simple analytic model

6.2.1.1 The valve-less diffuser pump - a vibrating mechanical system

The basic element in the valve-less diffuser pump is shown in Fig. 6-13. Very simplified, this can be seen as a Helmholtz resonator or as a mass-spring system. In the latter case, the spring is the diaphragm and the mass is mainly the mass of the fluid in the diffuser elements. Such a system is illustrated in Fig. 6-14 where also viscous damping is included. Like all systems possessing mass and elasticity it is capable of free vibration, i.e. it has natural frequencies. When such a system is subject to harmonic excitation it is forced to vibrate at the same frequency as the excitation frequency. When a system is excited by a transient force the resulting excitation take place at the natural frequencies of the system with the amplitude varying depending on the excitation. A mechanical system with one degree of freedom, x, and harmonic excitation is described by the differential equation [47]

$$m\ddot{x} + c\dot{x} + kx = F_0 \sin \omega t \tag{6-11}$$

where m is the mass, c is the viscous damping, k is the stiffness and $F = F_0 \sin(\omega t)$ is a harmonic force.

The solution to the homogeneous part decays exponentially with time and is only initially significant. The particular solution is a steady state oscillation of the same frequency as the excitation and it can be assumed to be of the form

$$x = X \sin(\omega t - \phi) \tag{6-12}$$

where X is the amplitude of oscillation and ϕ is the phase of the displacement with respect to the exciting force. By introducing $\omega_n = \sqrt{k/m}$, the natural frequency of undamped oscillation, $c_c = 2m\omega_n$, the critical damping, and $\zeta = c/c_c$, the damping factor, the nondimensional expressions for the amplitude and phase then become [47]

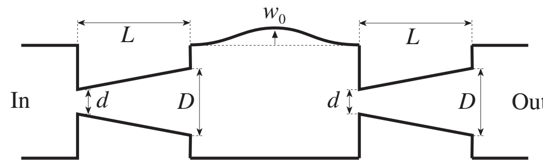

Fig. 6-13. A single chamber diffuser pump.

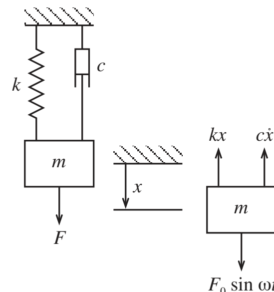

Fig. 6-14. Viscously damped system with harmonic excitation.

$$\frac{Xk}{F_0} = \frac{1}{\sqrt{\left[1-\left(\frac{\omega}{\omega_n}\right)^2\right]^2 + \left[2\zeta\left(\frac{\omega}{\omega_n}\right)\right]^2}} \tag{6-13}$$

and

$$\tan\phi = \frac{2\zeta \cdot \omega/\omega_n}{1-\left(\omega/\omega_n\right)^2}. \tag{6-14}$$

The solutions are plotted in Fig. 6-15. The curves show that the damping factor has a strong influence on the amplitude and phase angle for frequencies near resonance. The amplitude at the resonance can from Eq. (6-11) be found to be

$$X = F_0/c\omega_n = F_0/2\zeta k \tag{6-15}$$

Fig. 6-15 shows the impact that the resonance has on a vibrating mechanical system. A resonator with low damping is very effective in transforming input energy into a large vibration. This is used in the valve-less diffuser pump. Other examples of desired resonances are resonances in acoustical systems such as musical instruments or the human voice. An example is the vibration in a violin or piano string. More common is that resonance is to be avoided. To prevent large amplitudes from developing, dampers and absorbers are often used. Mechanical resonance is known to have built up to proportions large enough to be destructive. An example is the destruction of the Talcoma Narrows Bridge in 1940 [48]. Spacecraft, aircraft, and surface vehicles must be designed so that vibrations caused by their engines or by their movement through the air are kept to a safe minimum level.

The resonance frequencies for a system with low damping can be calculated assuming a conservative system. The total energy is then constant. For the free vibration of an undamped system, the energy is partly kinetic and partly potential. The kinetic energy is stored in the mass by virtue of its velocity, whereas the potential energy is stored in the from of strain

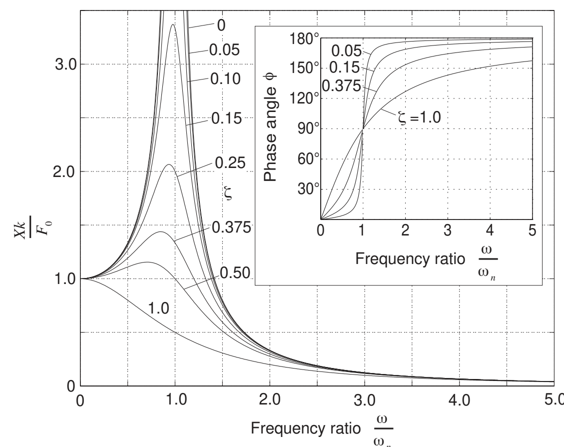

Fig. 6-15. Plots of the nondimensional equations for amplitude and phase versus ω/ω_n for different values of the damping factor, ζ.

energy in elastic deformation or work done in a force field such as gravity.

An approximate value of the resonance frequency of the diaphragm oscillation can be calculated using the mass-spring analogy where the elastic properties of the diaphragm represents the spring and the oscillating fluid in the diffuser elements represents the mass. Assuming a conservative system the energy will oscillate between the maximum potential energy of the diaphragm and the maximum kinetic energy of the fluid. The resulting resonance frequency f_0 for a single chamber pump with flat-walled diffuser elements with notations as in Fig. 6-13 is

$$f_0 = \frac{1}{2\pi}\left[\frac{K_p\left(1+\eta^{1/2}\right)^2 b(D-d)}{\rho K_v(1+\eta)L\ln\frac{D}{d}}\right]^{1/2} \tag{6-16}$$

where K_p and K_v are constants and b is the depth. This is described in detail in paper 1.

6.2.1.2 The continuity equation

A problem with the design of the diffuser pump is that, as far as the author knows, no analytic expression exists for the diffuser performance in the flow region in which this pump operates. Normally, in classic fluid mechanics diffuser design is based on experimental data and the pressure drops are expressed as in Eqs. (6-2) and (6-3).

At the resonance frequency the cavity volume variation due to the oscillating diaphragm can be expressed as

$$V_c = V_0 \sin 2\pi f_0 t \tag{6-17}$$

where

$$V_0 = K_v x_0 \tag{6-18}$$

there V_0 is the volume variation amplitude, K_v is a constant, x_0 is the diaphragm center deflection amplitude, f_0 is the pump excitation frequency and t is the time. Assuming that the pressure loss coefficients defined in Eq. (6-3) are constant it is possible to integrate over a complete pump cycle. Then an approximate expression for the net volume transport, Φ, for a single chamber with one diaphragm can be obtained at zero pump pressure across the pump as

$$\Phi = 2f_0 K_v x_0\left(\frac{\eta^{1/2}-1}{\eta^{1/2}+1}\right) \tag{6-19}$$

where $\eta = \xi_{nozzle}/\xi_{diffuser}$, i.e. the ratio of the pressure loss coefficients of the nozzle and the diffuser. The equation shows that the pump flow is maximized if η is maximized.

Recently the analysis was further extended to include pressure head and the chamber pressure [49]. Unfortunately analytic solutions are only possible for very simplified cases. The work presents some interesting results but inertial effects were not included. Consequently the relation between geometrical changes and the following change of the resonance frequency was not considered.

This analysis is presented in paper 1.

6.2.2 An electrical analogy used for designing a gas pump

The use of electrical analogies has been popular for micropumps. In Fig. 6-16 such a circuit used to design a gas pump is shown. The physical system is described by mechano-acoustical characteristic parameters which are used as equivalent electrical impedances [50]. With the viscous losses assumed to be zero the compressible gas pump system was found to have the resonance frequencies

$$\omega_{01}^2 \approx \frac{1}{(C_k + C_m)M_d} \text{ and } \omega_{02}^2 \approx \frac{1}{C_m M_m} + \frac{1}{C_k M_m} \tag{6-20}$$

where C_m and M_m are the equivalent double diaphragm and piezoelectric disc compliance capacitance and mass, M_d is the equivalent diffuser mass and C_k is the equivalent gas compression capacitance. The values of C_m, $M_{m,}$ M_d and C_k are given in Table 6-1 and the resulting theoretical and calculated pump diaphragm resonance frequencies are tabulated in Table 6-2. The higher resonance frequency is shown to give much higher pump flow amplitude than the low resonance frequency for the gas pump, while the low resonance frequency is used for a gas pump. The net pump flow and the pump cavity pressure can be written as

$$\Phi \approx 2V_0 \frac{\sqrt{C_m M_m}}{C_k M_d} \cdot \frac{1}{\pi} \cdot \frac{\eta^{1/2} - 1}{\eta^{1/2} + 1} \tag{6-21}$$

and

$$p_{c0} \approx \frac{V_0}{C_k} \tag{6-22}$$

where V_0 is the volume displacement amplitude.

This is described in detail in paper 6.

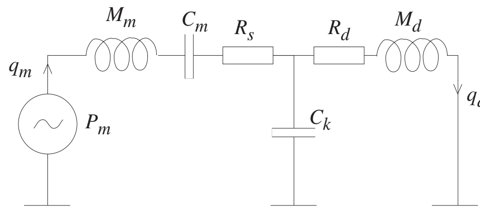

Fig. 6-16. An electrical analogy circuit of the diffuser gas pump at zero pump pressure. P_m is the equivalent piezoelectric disc excitation pressure, q_m is the volume flow due to the diaphragm displacement and q_d is the total volume flow in the two diffusers. Indices m, d and k are used to denote the different equivalent resistances, inductances and capacitances of the diaphragm, diffuser and cavity, respectively. The squeeze film flow resistance, R_s, and the diffuser flow resistance, R_d, were assumed to be zero.

Table 6-1. Constants and equivalent electrical impedances of the diffuser gas pump.

Parameter	Notation	Value	Unit
Air density	ρ	1.18	kg/m^3
Air compressibility	κ	$7.14\cdot10^{-6}$	m^2/N
Diaphragm resonance frequency in vacuum	f_o	10.3*	kHz
Diffuser element efficiency ratio ξ_n / ξ_d (assumed)	η	2	-
Total equivalent diaphragm compliance capacitance	C_m	$1.23\ 10^{-14}$*	m^3/Pa
Equivalent cavity compression compliance capacitance	C_k	$8.08\cdot10^{-14}$*	m^3/Pa
Total equivalent diaphragm mass	M_m	$1.94\cdot10^{4}$	kg/m^4
Total equivalent diffuser mass	M_d	$1.4\cdot10^{5}$	kg/m^4

* Calculated using ANSYS FEM-simulation.

Table 6-2 Theoretical and measured pump diaphragm resonance frequencies.

Res. frequency	Medium	Theory (kHz)	Measurement (kHz)	Comment
$f_{o,vac}$	Vacuum	10.3*	10.8	*ANSYS-simulation
f_{o1}	Air	1.4	~1.5	Very low amplitude
f_{o2}	Air	11.1	11.2	Very high amplitude

6.2.3 A lumped-mass model

To optimize the valve-less diffuser pump a model is necessary that sufficiently describes the system. The model must include stiffness, masses and viscous losses and be able to handle nonlinearities. For simplified cases it is possible to set up an analytic model, but mostly numerical methods are needed for realistic systems.

One possibility is to use a finite element program. The problem is that for most realistic systems the finite element models are to large to be possible to solve even using today's powerful computers. The usual approach is instead to use a lumped-mass model to describe the system. The system is divided into lumped mass elements which can be described individually by simple analytic models and for which simple relations between the different elements can be formulated [2]. The approach has previously been used for other micropumps [32, 51-53].

In its simplest form the valve-less diffuser pump consist of a pump chamber with a diaphragm and two diffuser elements as illustrated in Fig. 6-17. The diffusers are connected in series with flow channels. The pressures at the inlet and the outlet are assumed constant.

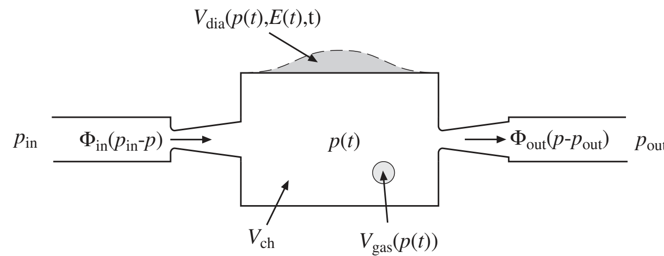

Fig. 6-17. A drawing of the basic unit in a valve-less diffuser pump.

An equation for the diaphragm can be formulated using Newton's second law. For the pumps tested with liquids it can be shown that the mass of the diaphragm is negligible compared with the other masses in the system and the equation can be written as

$$\frac{dV_{dia}}{dt} = \frac{\partial V_{dia}}{\partial E} \cdot \frac{dE}{dt} + \frac{\partial V_{dia}}{\partial p} \cdot \frac{dp}{dt} \qquad (6\text{-}23).$$

where V_{dia} is the volume change due to deflection of the diaphragm, p is the chamber pressure, E is the electric field strength across the piezoelectric disc used for the actuation and t is the time.

The conservation of mass law can be used on the chamber volume. Assuming a stiff chamber and that the chamber volume, V_{ch}, is much larger than the volume change due to the deflection of the diaphragm the equation can be written

$$\frac{dp}{dt} = \frac{F_{in}(p_{in} - p) - F_{out}(p - p_{out}) - \frac{\partial V_{dia}}{\partial E} \cdot \frac{dE}{dt}}{\frac{\partial V_{dia}}{\partial p} + k_{liquid} V_{ch} + \left(\frac{1}{p + p_0} - k_{liquid}\right) \cdot \frac{x \cdot V_{ch} \cdot p_0}{p + p_0}} \qquad (6\text{-}24)$$

where Φ_{in} is the flow through the inlet, p_{in} is the pressure at the inlet, Φ_{out} is the flow through outlet, p_{out} is the pressure at the outlet, κ_{liquid} is the compressibility of the liquid

which is assumed constant, p_0 is the pressure outside the chamber and x is the relative gas content (V_{gas}/V_{ch}) in the chamber at the pressure p_0. The gas is assumed to be ideal. The properties of the diaphragm were calculated using the finite element program ANSYS®.

A flow channel of arbitrary shape can be analyzed using the energy equation for a fixed control volume. For a channel where the flow can be assumed one dimensional and for which the cross-sectional areas and velocity profiles at inlet and outlet are the same the equation can written

$$p_{in} = p_{out} + \rho\alpha\frac{d\Phi}{dt} + \Delta p_{loss} \qquad (6\text{-}25)$$

where α depends on the velocity profile and Δp_{loss} is the pressure drop due to viscous losses. Assuming a flat flow profile the factor α for a channel with constant cross-sectional area, A, is

$$\alpha = \frac{L}{A} \qquad (6\text{-}26)$$

where L is the length of the channel.

The equation system is illustrated as an electric circuit in Fig. 6-18. It was solved using MATLAB® and the equation system can easily be extended for other configurations including more chambers, buffer elements and flow channels.

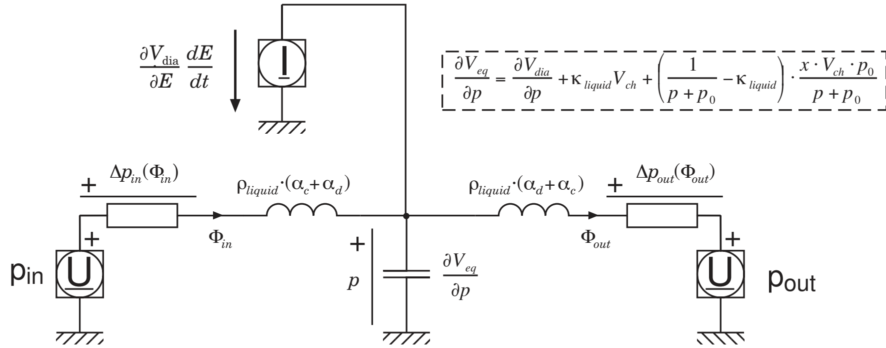

Fig. 6-18. A electric circuit illustrating the simplest form of the valve-less diffuser pump. Inertial effects in the diaphragm and chamber and viscous losses in the chamber are neglected.

The flow losses in the diffuser elements are taken form steady flow measurements of the flow-pressure characteristics. Using a least square fit of a polynomial the measured pressure, $\Delta p_{\text{measured}}$, was expressed as

$$\Delta p_{\text{measured}} = \begin{cases} k_1\cdot\Phi + k_2\cdot\Phi^{7/4} & ,\Phi \geq 0 \\ k_3\cdot\Phi + k_4\cdot\Phi^{7/4} & ,\Phi < 0 \end{cases} \qquad (6\text{-}27)$$

where Φ is the flow and k_1, k_2, k_3 and k_4 are the coefficients of the least square fit. The fitted functions showed very good agreement with the measured values.

For a dynamic flow situation the losses can be expected to be different. To account for this and other effects not described by the model equation (6-27) was changed to

$$\Delta p_{\text{model}} = \begin{cases} C_1 \cdot \left(k_1 \cdot \Phi + k_2 \cdot \Phi^{7/4}\right) & ,\Phi \geq 0 \\ C_2 \cdot \left(k_3 \cdot \Phi + k_4 \cdot \Phi^{7/4}\right) & ,\Phi < 0 \end{cases} \tag{6-28}$$

where C_1 and C_2 are two coefficients to be fitted based on the measured flow-pressure characteristics during pump operation.

The flow losses, Δp, of other parts were calculated using the law of friction for laminar flow [46]

$$\Delta p = \frac{1}{2} \frac{c}{D_h^2} L \cdot \eta \cdot \overline{u} \tag{6-29}$$

where c is a parameter depending on the geometric shape, L is the channel length, η is the viscosity, $\overline{u}$ is the mean velocity and D_h is the hydraulic diameter. The latter is calculated as

$$D_h = \frac{4 \cdot \text{Area}}{\text{wetted perimeter}} \tag{6-30}$$

For flow through a circular cross-section c can be determined analytically to be 64. For rectangular cross-sections data can be found in the literature [4] and fitted to a polynomial using the least square method:

$$c = 95.96 - 128.49 \cdot \frac{a}{b} + 171.78 \cdot \left(\frac{a}{b}\right)^2 - 116.54 \cdot \left(\frac{a}{b}\right)^3 + 34.206 \cdot \left(\frac{a}{b}\right)^4 \tag{6-31}$$

Here a and b are the side lengths with $a \leq b$.

This is described in detail in paper 8.

6.3 Diffuser pump fabrication techniques

The diffuser pump principle is general and not limited to any specific fabrication technique. Pumps have been fabricated using different techniques and dimensions in metal, silicon/glass and plastic. The metal pump has the advantage of fast prototype fabrication. The fabrication of a pump in silicon is a more complicated process. The advantage is that many pumps can be fabricated at the same time. The use of silicon and glass have also advantages over metals as pump materials, e.g. in applications with an aggressive medium a silicon/glass pump may be more resistant than a metal pump. The use of the thermoplastic polycarbonate as pump material has the advantage that the material is inexpensive compared with more commonly used materials in MST. Based on one master it is possible to fabricate thousands of pumps. The main disadvantage of polycarbonate, and most other plastics, is that it is very flexible, which may result in less stiff pump designs and thus poorer pump performance.

6.3.1 Conventional technologies

Today there exist conventional technologies for the fabrication of structures in the size ranges of tens of micrometers. The first fabricated pump was made in brass with conventional techniques. A cross-sectional drawing is shown in Fig. 5-8 [20]. It was designed for water but was shown to work for both water and air. A larger, electromagnetically driven pump shown in Fig. 6-19 has also been built and tested [54]. It was designed to have a diaphragm pump resonance frequency optimized for line frequency (50 Hz). This pump, with a pump chamber diameter of 44 mm, had a maximum flow rate of 1.8 l/min and a maximum pump pressure of 3 m H_2O.

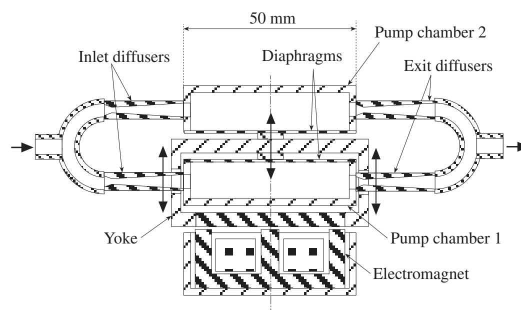

Fig. 6-19. Cross-sectional view of the electromagnetically driven two-chamber pump [54].

The planar metal pump presented in paper 1 is fabricated from 0.5 mm thick plates of brass into which the pump chamber cavities and diffusers were milled to a depth of 0.15 mm in one milling sequence. A top view and a photo of the pump are shown in Fig. 6-20. The pump chamber diameter is 13 mm and the diffuser inlets are slightly rounded with a throat width of 0.3 mm and a diffuser outlet width of 1.0 mm. The diffuser length is 4.1 mm. The resulting diaphragm thickness was 0.35 mm. Four PZT-piezoelectric discs 10 mm in diameter and 0.2 mm thick were fixed to the four pump diaphragms using adhesive.

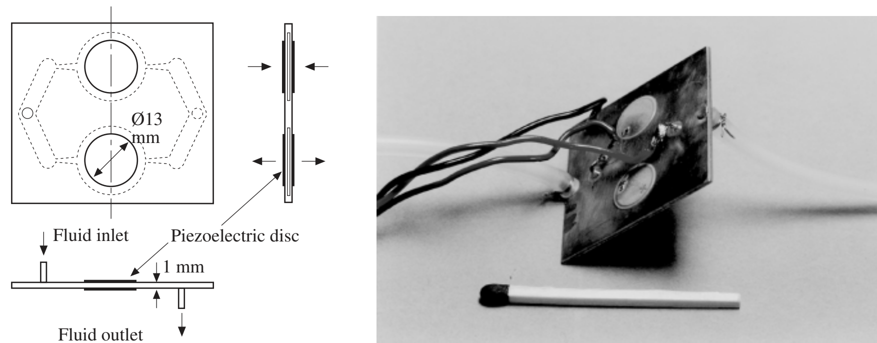

Fig. 6-20. The valve-less planar metal (brass) pump with two pump chambers.

The metal pump designed for gas presented in paper 6 was fabricated in brass using conventional methods. The design with dimensions is shown in Fig. 6-21a and the mounting of the pump is shown in Fig. 6-21b. The diffusers are of the flat-walled type with length 3 mm, depth 0.1 mm, inlet width 0.12 mm and outlet width 0.64 mm. The resulting opening angle is 10°. The pump has two large-area, in-phase operated diaphragms (Ø12 mm) arranged on either side of the pump cavity. Piezoelectric discs (Ferroperm, Pz 26) were glued to each pump diaphragm for the excitation. A photo of the assembled pump is shown in Fig. 6-22.

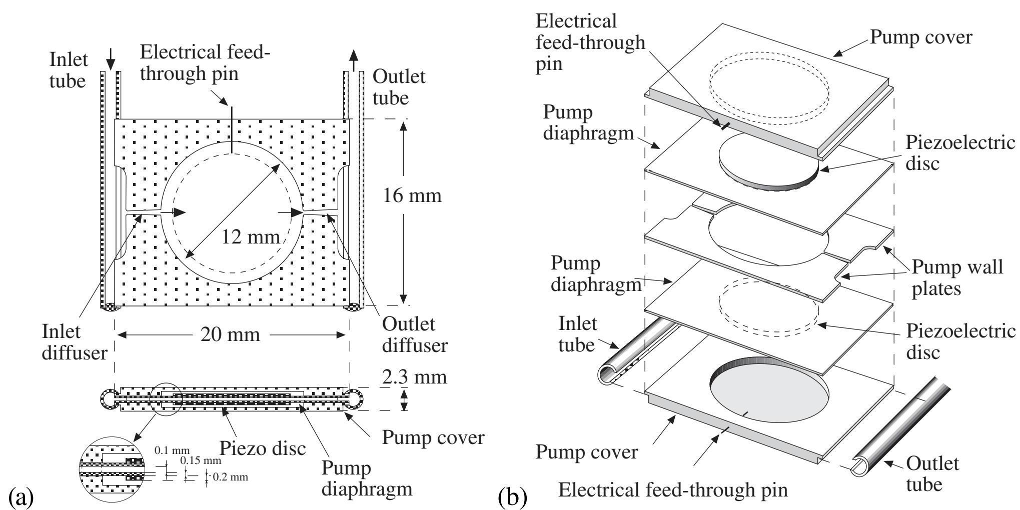

Fig. 6-21. The valve-less metal (brass) pump designed for gas pumping: (a) the dimensions of the pump unit and (b) an exploded view of the design.

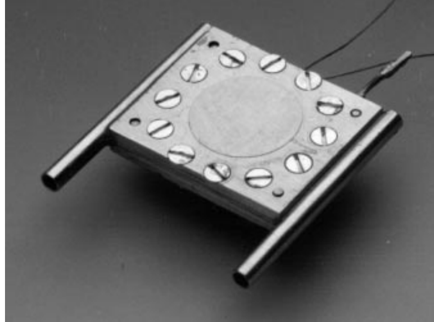

Fig. 6-22. A photo of the valve-less metal (brass) pump designed for gas pumping.

6.3.2 Micromachining

It is possible to further scale down the diffuser pump by using micromachining technology. The most often used material is silicon which can be micromachined using wet or dry etching. For sealing it is common to use glass bonded to silicon. Attempts have also been made to use other techniques, e.g. electroplating of high permeability nickel-iron permalloy [21] and thermoplastic molding [10].

6.3.2.1 Silicon micromachining

A valve-less diffuser pump fabricated using isotropic wet etching

The first micromachined version of the diffuser pump was fabricated using isotropic wet etching. The basic process steps are shown in Fig. 6-23. The pump was fabricated in a 500 μm thick silicon wafer of <100> type polished on both sides. Pump, inlet and outlet cavities and diffuser elements were etched using a two-step isotropic HF-HNO_3-CH_3COOH etch (HNA). Fluid inlet and outlet openings, saw lines and marks for the piezoelectric drive discs were etched from the other side using anisotropic KOH etching. The pumps were sealed by a glass wafer anodically bonded to the silicon wafer. This resulted in diffuser elements with "half-elliptic" cross-sections at the diffuser throat and "half-oval" cross-sections at the diffuser outlet. The pump chip was 15×18 mm with a thickness of 1 mm. Piezoelectric drive discs (Philips, PXE5) 0.2 mm thick and 3.8 mm in diameter were glued using conductive epoxy to the pump diaphragms and brass tube connectors were glued to the inlet and outlet holes of the pumps. The pump chambers have diameters of 6 mm. The diffuser dimensions are summarized in Table 6-3 for three tested pumps. Photos of a pump unit are shown in Fig. 6-24. The work is presented in papers 2 and 3.

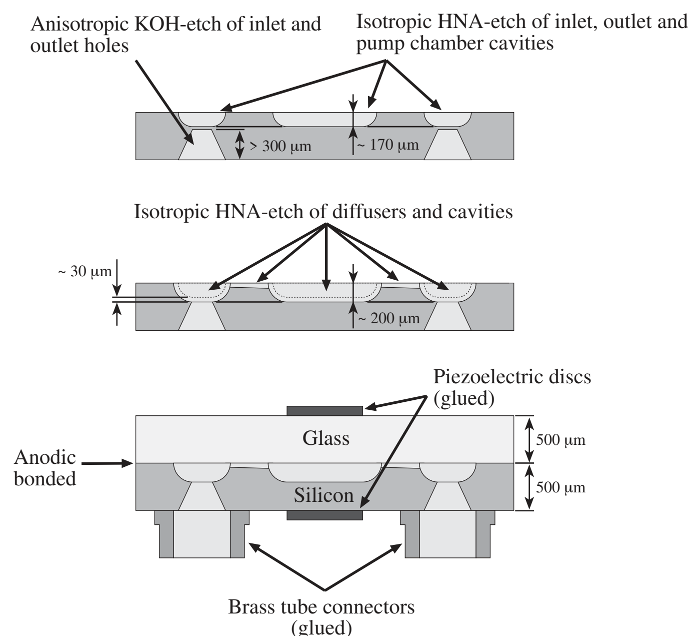

Fig. 6-23. The process used for the isotropic etched valve-less diffuser pump.

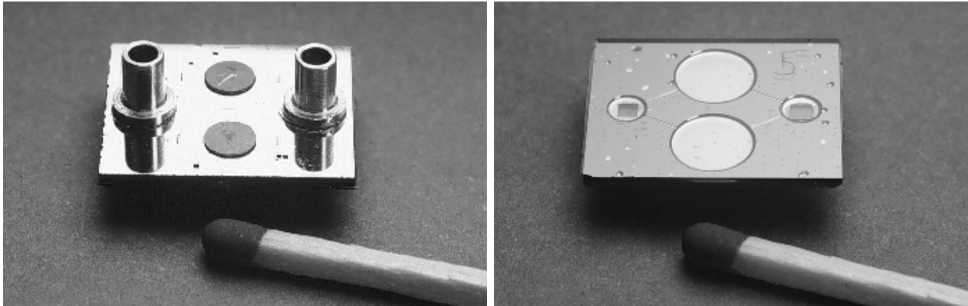

Fig. 6-24. Photos of the isotropic etched pump from the silicon side and the glass side.

Table 6-3. Diffuser dimensions for three different isotropically etched pump units.

Diffuser length [μm]	Throat width [μm]	Outlet width [μm]	Diffuser depth [μm]	Diffuser angle
1450	94	204	27-31	4.2°
2450	92	283	28-33	4.5°
3250	100	341	31-38	4.2°

A pump fabricated using deep reactive ion etching

The rapid development of the technology for reactive ion etching (DRIE) during recent years opens new possibilities for microfabrication of the valve-less diffuser pump. Arbitrary planar design is possible and control of the diffuser dimensions is significantly improved compared to the isotropic etch used for the first micromachined valve-less diffuser pump. It is also possible to fabricate the diffusers with rectangular cross-sections, which can be made shorter than conical-diffusers with the same performance [4]. This can be utilized to make smaller pumps. The fabrication process is straightforward; it consists of only two masks and one step with deep reactive ion etching for the pump cavities and diffuser elements and one step with

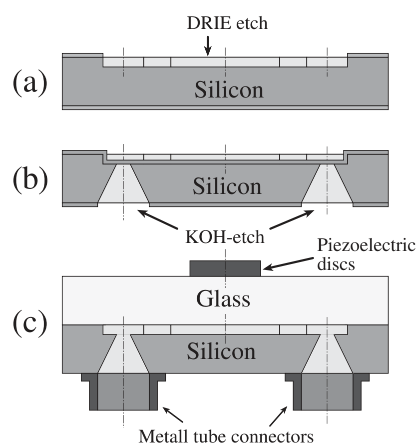

Fig. 6-25. The process used for the DRIE-pumps.

anisotropic KOH etch for the inlet and outlet openings. The basic process steps are shown in Fig. 6-25. The silicon wafer is anodically bonded to a glass wafer and sawed into 15×17 mm pump chips. Piezoelectric discs are glued to the glass diaphragms for excitation of the pump. Photos of a pump unit are shown in Fig. 6-26 and the dimensions of the tested pumps are given in Table 6-4. The deep silicon etching was done by Alcatel CIT and Surface Technology Systems Ltd. (STS). The work is presented in papers 4 and 7.

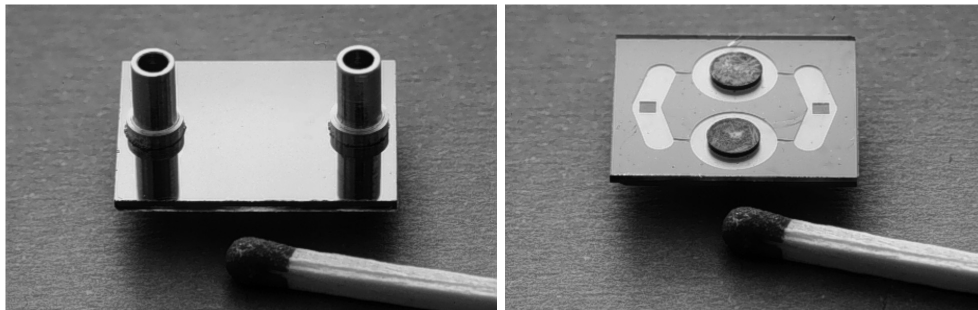

Fig. 6-26. Photos of a DRIE pump showing the silicon side and the glass side. The size of the pump chip is 15×17×1 mm^3 and the chamber diameter is 6 mm.

Table 6-4. Dimensions of the tested DRIE pumps (80 μm depth).

Diffuser throat width [μm]	Diffuser length [μm]	Length to throat width ratio	Diffuser angle
20	273	13.7	9.8°
40	547	13.7	9.8°
40	720	18.0	9.8°
40	1000	25.0	9.8°
80	1093	13.7	9.8°
80	1440	18.0	9.8°
80	1093	13.7	7.0°
80	1093	13.7	13°

6.3.2.2 Thermoplastic replication

The planar geometry of the deep reactive ion etched silicon pump makes it very suitable for thermoplastic replication. The potential of high volume production at low cost makes this very promising since the costs per pump should be significantly reduced compared with the silicon pumps. Two different thermoplastic replication technologies were tested: injection molding and hot embossing. The main process steps are shown in Fig. 3-6. First a master structure is fabricated using a high-precision micromachining technique. In Fig. 3-6 deep reactive ion etching of a photolithographically defined pattern is used, but other methods are also possible, e.g., wet etching or the LIGA process. A negative mold insert is then fabricated from the master using electroplating. The mold insert is used in the injection molding or hot embossing process where a large number of plastic replicas are fabricated. The design of a pump replicated

from a deep reactive ion etched master structure is shown in Fig. 6-27a and a photo of an 80 μm deep injection molded pump is shown in Fig. 6-27b. The injection molding was done in a commercial injection-molding machine for CD-manufacturing. From one properly made nickel mold insert it is possible to fabricate more than 10 000 plastic discs with a diameter of 80 or 120 mm. The cycle time for one disc is less than 10 seconds and the plastic material cost is about 5 cents per disc. In order to test the injection-molding process for deep structures, brass mold inserts were fabricated with depths up to 0.2 mm using a NC workshop milling machine. They were used successfully as master structures in the injection molding machine.

The work is presented in paper 5.

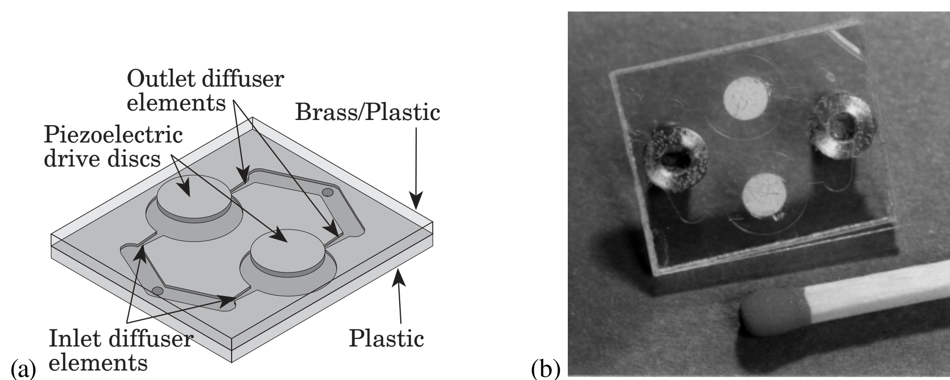

Fig. 6-27. (a) A perspective view of a valve-less diffuser double-chamber micropump fabricated using thermoplastic replication and (b) a photo of a mounted injection molded pump fabricated in polycarbonate (chip size for both pumps 15×17×1.4 mm^3).

6.4 Results from experiments and simulations

Extensive measurements have been made to evaluate and characterize the valve-less diffuser pumps. Both passive measurements and pump performance measurements have been made. The measurements have been compared with simulations in order to evaluate the pump and improve the design.

6.4.1 Liquid pumping

6.4.1.1 Steady flow characteristic

The flow resistances for complete pump units and single diffuser elements have been measured to understand the influence of the diffuser design . The measurements were done by applying a static pressure across the unit and measuring the flow through it. For small pressures a water column was used to apply the pressure and for higher pressures pressurized nitrogen was used to force the liquid through the diffuser element. The measurements show that there exists a flow directing effect of the diffuser elements also for small flows. For small flows there is an indication that the flow is nearly laminar, but as the flow increases other effect such as turbulence have to be taken into account. A typical example of the flow-pressure characteristic is shown for the pump in paper 1 in Fig. 6-28. Measurements for other pumps are presented in paper 3 and 7.

The CFD-program ANSYS/FLOTRAN was used in paper 7 to simulate the flow-pressure characteristics for diffuser elements of the same type as used in the deep reactive ion etched pumps in paper 4. The results form the simulations were compared with experimental

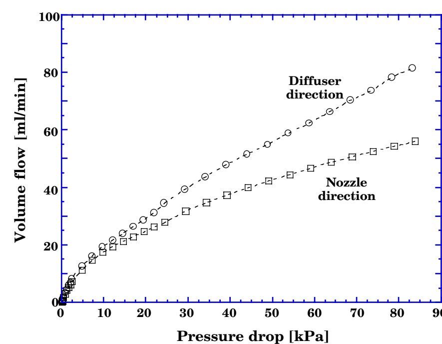

Fig. 6-28. Flow-pressure characteristic for steady flow for the double-chamber brass pump in paper 1.

Table 6-5. Measured and simulated diffuser element efficiency ratios, η, for water. The diffusers elements are flat-walled with the depth 80 µm. The analysis values are for the conical diffuser element in Fig. 6-7.

Element type	W1 [µm]	L [µm]	L/W1	α	Steady flow η				Pump performance	
					Measured	2D laminar	3D laminar	Analysis	Max. flow [µl/min]	Max. pressure [m H_2O]
3a	80	1093	13.7	9.8°	1.43	2.08	1.18	3.6	1946	5.44
3b	80	1440	18.0	9.8°	1.51	2.24	1.48	3.6	1285	2.44
3c	80	1093	13.7	7.0°	1.59	1.88	1.35	3.6	2270	7.57
3d	80	1093	13.7	13°	1.33	3.20	1.75	3.6	2218	4.71

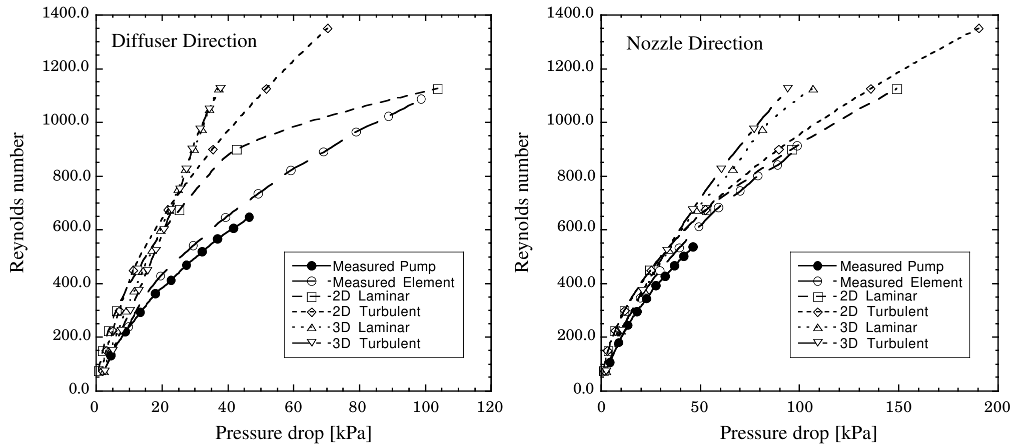

Fig. 6-29. Measured and simulated flow-pressure characteristics for a diffuser element with a throat cross-section of 80×80 μm², a length of 1.093 mm and an opening angle of 9.8°.

determined flow-pressure characteristics for single diffuser elements. The geometrical dimensions of the diffuser elements and the simulated diffuser element efficiency ratios are given in Table 6-5. The simulated flow-pressure characteristic for a diffuser element with a throat cross-sectional area of 80×80 μm², an opening angle of 9.8° and a length of 1.093 mm is compared with the experimentally determined flow-pressure characteristics in Fig. 6-29. The simulations show that the diffuser element has flow directing capability in the diverging-wall direction but the result is not accurate enough to use for design optimization. The three-dimensional model predict the flow well for low Reynolds numbers, but the discrepancy grows with increased Reynolds number. For the whole measured pressure region the two-dimensional model shows good agreement with the measurements in the nozzle direction, while the discrepancy is larger in the diffuser direction. Comparison with the other simulated elements indicates that the difference between simulations and measurements is smallest for the smallest angle and largest for the largest angle. No significant difference is seen between the turbulent and the laminar solutions for the simulated flow-pressure characteristics in Fig. 6-29. The exception is the two-dimensional model for Reynolds numbers greater than 900 in the diffuser direction. The reason is that a large backflow occurs for the laminar solution.

It is important to be aware of that the steady state flow-pressure characteristic may differ from the flow-pressure characteristic during dynamic conditions. From macroscopic fluid dynamics it is known that the flow pattern for a dynamic situation differs significantly from a steady state situation as illustrated in Fig. 6-30. It is also known that the transition from laminar to turbulent flow is affected [46].

This is presented in papers 1, 3 and 7.

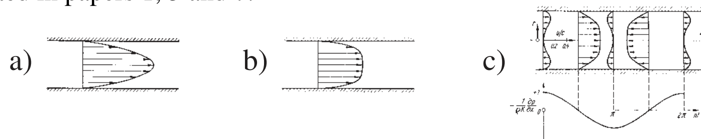

Fig. 6-30. The velocity profile for fluid flow in a pipe under (a) steady state laminar conditions, (b) steady state turbulent conditions and (c) dynamic laminar conditions [46].

6.4.1.2 Pump performance

Pumps of different sizes and with different diffuser geometries have been tested and characterized. The volume flow and the pressure head were measured during the measurements. Depending on the size of the pump flow it was measured either by a scale connected to a computer (paper 1) or by measuring the movement of the liquid surface in a tube of known diameter (paper 2, 4 and 5). The pressure head was measured using a water column for the pumps with maximum pressure head below 20 kPa. For pumps with higher pressure heads a commercial pressure sensor (Motorola MPX100, 0-100 kPa, ±0.05% Full Scale Linearity) was used. The set-up used for the pressure sensor is shown in Fig. 6-31.

Performance was good for all pumps compared to other micropumps. The maximum volume flow can easily be varied by changing the cross-sectional area of the diffusers in the pumps. Diffuser pumps with maximum volume flows ranging between 42 μl/min and 16 ml/min are presented in papers 1 to 4. A diffuser pump has also been fabricated which shows a

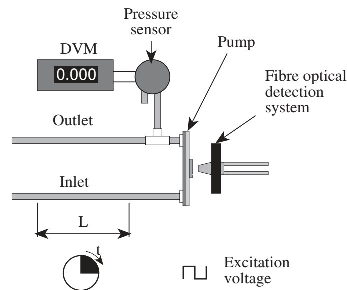

Fig. 6-31. Measurement set-up for the pump performance measurements in paper 4.

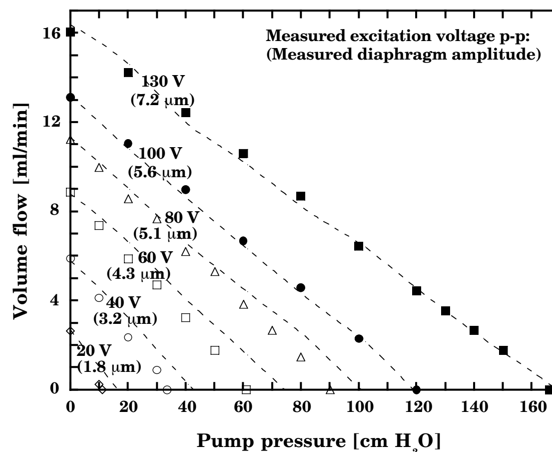

Fig. 6-32. Measured and calculated flow-pressure characteristics for the two-chamber brass pump for water in anti-phase operation for different excitation voltages (and diaphragm amplitudes at zero pump pressure). The calculated values are from the simple model with one chamber with the calculated flow doubled. The symbols indicate the measured values and the dashed lines show the simulated results. The resonance frequency was 540 Hz for the experiments (paper 1) and 600 Hz for the simulations (paper 8).

maximum volume flow of 1.8 l/min [54]. Thus the highest maximum flow rate is 40 000 times the lowest maximum flow rate. For a specific pump unit the volume flow can be controlled by changing the excitation voltage. This is shown in Fig. 6-32 (paper 1). The first micromachined diffuser silicon pumps presented in paper 2 are interesting since they show that the valve-less diffuser pump principle works also for the strange ”half-elliptic” cross-section with as small dimensions as 30×100 µm.

In paper 4 several different pumps with different diffuser geometries were compared. It was clearly shown that diffuser design is important for pump performance. To optimize the pump performance it is necessary to know the type of liquid. The results are presented in Table 6-6. Especially noteworthy is the high pressure head achieved. The maximum pressure head of 74 kPa is one of the better presented for micropumps. In Fig. 6-33 the measurements for the pump unit with highest pressure head for water are presented.

The measurements on the plastic pumps in paper 5 indicate that a stiff pump structure is important. Several different plastic pumps were tested. There was a significant difference in the pump performance if the pump was clamped in a stiff metal structure or not. The resonance frequency was only 20 % higher for the clamped pump compared with the best non-clamped pump, but the pump flow increased by a factor 4 and the pump pressure by a factor 5.

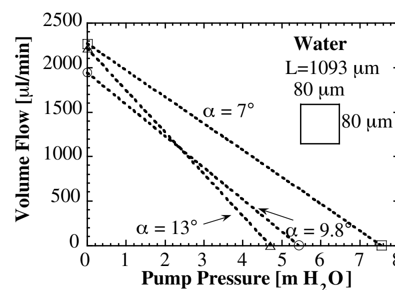

Fig. 6-33. Water volume flow vs. pump pressure characteristic for a silicon diffuser pump with 80×80 µm diffuser throat cross-section and different opening angles, α.

Table 6-6. Pump performance for 80 µm deep DRIE pumps.

Pump	W1 [µm]	L [µm]	L/W1	α	Diaphragm amplitude [µm] Methanol	Max. flow [µl/min]	Max. pressure [m H_2O]	Diaphragm amplitude [µm] Water	Max. flow [µl/min]	Max. pressure [m H_2O]
1a	20	273	13.7	9.8°	0.27	314	2.76	-	-	-
2a	40	547	13.7	9.8°	0.55	628	2.70	-	-	-
2b	40	720	18.0	9.8°	0.34	781	3.92	-	-	-
2e	40	1000	25.0	9.8°	0.40	1156	3.81	-	-	-
3a	80	1093	13.7	9.8°	0.66	2537	5.57	0.64	1946	5.44
3b	80	1440	18.0	9.8°	0.69	2900	5.58	0.39	1285	2.44
3c	80	1093	13.7	7.0°	0.68	2693	6.17	0.72	2270	7.57
3d	80	1093	13.7	13°	0.63	3427	6.00	0.58	2218	4.71

"-" Not measured.

The lumped-mass model in paper 8 were tested for several of the pumps. For each pump the simulation started with finding the frequency of maximum volume flow. Then the excitation level and the coefficients C_1 and C_2 in Eq. (6-28) were adjusted to fit the measured data. This was repeated until the result was satisfactory. In Fig. 6-32 the dashed lines shows the simulated flow-pressure characteristic for the double-chamber brass pump in paper 1. The simulations were done using a model with one chamber with the flow doubled to correspond to a double chamber pump driven in anti-phase. The excitation levels for the simulations were chosen to correspond to the measured volume flows. The volume flow and the pressure head were also calculated as a function of the diaphragm excitation frequency. The results are plotted in Fig. 6-34 together with experimental results. It shows that the valve-less diffuser pump works as a resonator with maximum for both the volume flow and the pressure head at approximately the same frequency. The simulated resonance frequency is slightly higher than the measured.

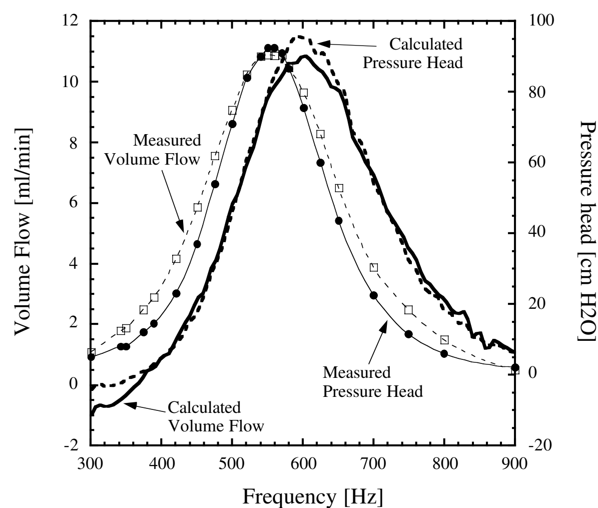

Fig. 6-34. Measured and simulated maximum flow at zero pressure head and maximum pressure head at zero volume flow for the double-chamber brass pump in paper 1. The excitation voltage was 80 V p-p for the measurements.

The lumped-mass model gives also possibility to study the pressure inside the pump chamber. The result for the highest excitation level is shown in Fig. 6-35 and indicates that absolute chamber pressure comes close to zero and that vaporization due to low chamber pressure probably is a problem. This is a parameter that limits the excitation level of the valve-less diffuser pump and for reliable pumping it is important to know where this limit is for a specific pump design.

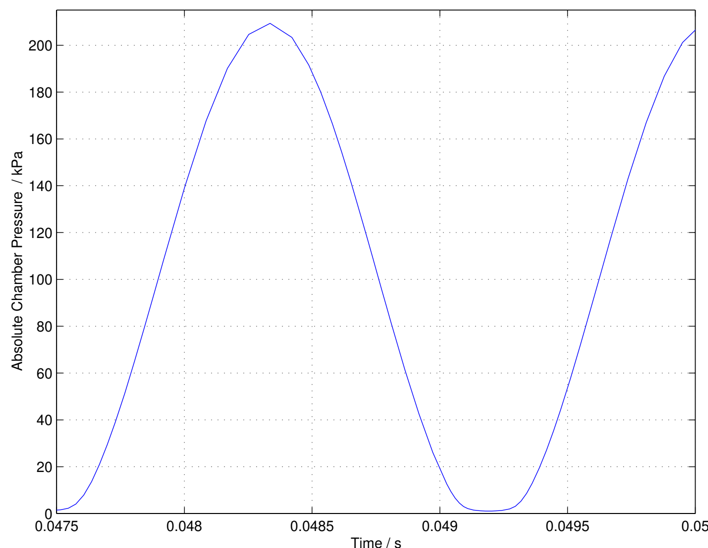

Fig. 6-35. The calculated chamber pressure inside the Flat-walled Brass Pump at the highest excitation level and zero pressure head. The calculated minimum pressure is about 0.6 kPa, i.e. below the vapor pressure.

The lumped-mass model in paper 8 was also used to investigate improved designs of the flat-walled silicon pumps in paper 4. One possible design is a serial pump with two chambers and three diffuser elements as shown in Fig. 6-36. Another possibility is to reduce the size of the diffuser elements. The results of the simulations are shown in Fig. 6-37. The steady flow-pressure characteristics of the diffuser elements was assumed to scale as between the flat-walled brass pump in paper 1 with 300×300 μm^2 throat cross-sectional area and the corresponding flat-walled silicon pump in paper 4 with 80×80 μm^2 throat cross-sectional area. The results shows that a serial pump with the chambers driven in anti-phase should almost double the attainable pressure head and also increase the maximum volume flow.

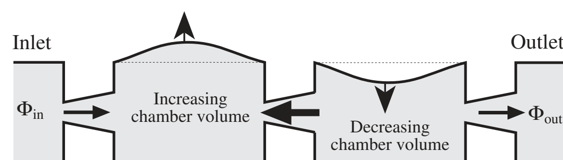

Fig. 6-36. A serial pump operated in anti-phase.

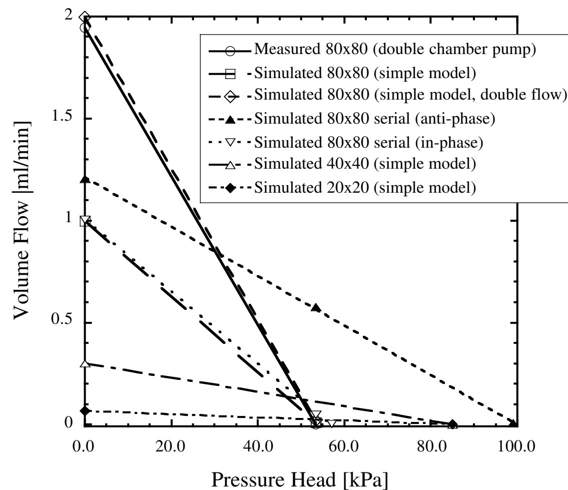

Fig. 6-37. Measured and calculated flow-pressure characteristics for the Flat-walled Silicon Pump. Calculations are also done for serial pumps and pump with reduced diffuser element sizes and depths. The measured pump had a resonance frequency of 3350 Hz. The simulated pump with 80×80 µm throat had 3500 Hz, that with 40×40 µm throat had 2650 Hz and that with 20×20 µm throat had 1619 Hz. The serial pump had a resonance frequency of 4260 Hz in anti-phase operation and 2440 Hz in in-phase operation.

6.4.2 Gas pumping

The theoretical and measured resonance pump frequencies are given in Table 6-2 and there is excellent agreement between them. Excitation at the low resonance frequency did not result in any measurable gas flow, while the high resonance frequency produced excellent pump flow results. The volume flow was measured using the time it took for a soap bubble to travel a known distance inside a glass tube connected to the pump outlet. The outlet pressure was measured using a pressure sensor. The measured pump flow is shown in Fig. 6-38 together with the theoretically calculated values.

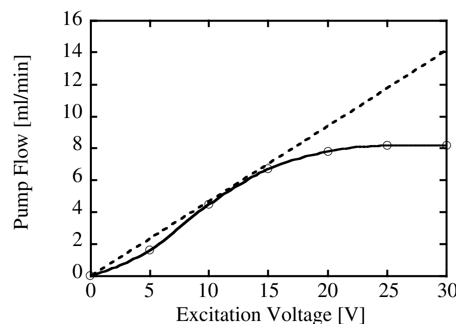

Fig. 6-38. Maximum pump air flow as a function of the excitation amplitude voltage at zero differential pump pressure. The straight line (dashed) represents the theoretically calculated flow based on a diffuser element efficiency, η=2. Eq. (6-19) was used for the calculation.

7 Summary of appended papers

The appended papers describe the principle of the valve-less diffuser pump, the design, the fabrication, measurements on different pump units and simulations. The papers are given in chronological order. Paper 1 presents the double-chamber pump milled in brass together with simplified theoretic expressions for its performance. Papers 2 and 3 presents pump and diffuser element measurements and analysis of the isotropically etched pumps. Paper 4 presents the deep reactive ion etched pumps. Paper 5 presents the pumps fabricated using thermoplastic replication. Paper 6 presents the gas pump. Paper 7 presents an experimental and numerical investigation of flat-walled diffuser elements and paper 8 presents a lumped-mass model of a valve-less diffuser pump.

Paper 1

A planar version of the valve-less diffuser pump is presented as a first step towards a micromachined version. The pump unit consists of two piezoelectrically actuated pump chambers, each with one flow directing flat-walled diffuser element at the inlet and one at the outlet. The pump chamber diameter is 13 mm and the diffuser/nozzle element throat dimensions are 0.3 × 0.3 mm. It is fabricated in brass with a total thickness of 1 mm. Simplified theoretical analyses of the maximum pump flow and resonance frequency are given. The flow directing ability of the diffuser elements is demonstrated in a stationary flow situation and the pump performance is tested in anti-phase and in-phase excitation. The measurements in the anti-phase mode show pump flows and pump pressures which were more than twice as high as those of the in-phase mode. A maximum volume flow of about 16 ml/min and a maximum pump pressure of about 1.7 m H_2O was measured in the anti-phase operation mode with the pump diaphragm vibration frequency set to 540 Hz.

Paper 2

The first micromachined version of the valve-less diffuser pump is presented. It is a planar double chamber pump isotropically etched in a silicon wafer anodically bonded to a glass wafer. The diffuser elements have a depth of 24 - 48 µm and a throat width of 88 - 104 µm. The pump chamber diameter is 6 mm. Pump cavities and diffuser elements are etched with an isotropic HNA silicon etch. Pumps with three different diffuser lengths are compared. They reach a maximum pump capacity of 230 µl/min and a maximum pump pressure of 1.7 m H_2O, both at a resonance frequency of 1318 Hz for methanol.

Paper 3

The flow directing properties of several micromachined diffusers of the types used in the pumps in paper 2 are investigated. Experimental results are compared with analytical results. The lengths of the diffusers are from 1.45 to 3.95 mm and the half-elliptic throat cross-sections about 30×100 µm.

Paper 4

Deep reactive ion etching (DRIE) is used to make valve-less diffuser pumps. The pumps were fabricated in a two mask micromachining process in a silicon wafer which then was anodically bonded to a glass wafer. Pump chambers and diffuser elements were etched in the silicon wafer using DRIE while inlet and outlet holes were etched using an anisotropic KOH-etch. The DRIE process makes it possible to have flat-walled diffuser elements. The maximum pump pressure attained is 7.6 m H_2O (74 kPa) and the maximum pump flow is 2.3 ml/min, both for water.

Paper 5

Thermoplastic replication is used to fabricate valve-less diffuser pumps. The simple planar geometry of the diffuser pump makes thermoplastic replication very attractive. Two different methods were tested: hot embossing and injection molding. We used 0.1 and 0.2 mm deep precision milled brass mold inserts and 20 and 80 μm deep microelectroformed nickel mold inserts defined from deep reactive ion etched (DRIE) silicon wafers. For the injection molding a commercially available Compact Disc injection molding machine (Toolex Alpha MD100) was used to fabricate the diffuser micropumps. The cycle times are short, less than 10 seconds per disc, and one properly fabricated mold insert of nickel can be used to fabricate more than 10,000 plastic discs. The plastic material cost is about 5 cents per disc. Tested pumps reached a maximum volume flow of 1.2 ml/min and a maximum pump pressure of 16 kPa.

Paper 6

The paper presents the first valve-less diffuser pump designed for gas pumping. An electrical analogy is used to calculate the pump resonance frequencies and the pump flow. The pump is fabricated in brass and has two flat-wall diffusers connected to a pump chamber with two diaphragms excited by piezoelectric discs. The pump dimensions are 20 × 16 × 2.3 mm. The measured maximum pump pressure and volume flow are 5 kPa (0.5 m H_2O) and 8 ml/min, respectively.

Paper 7

The Computational Fluid Dynamics program ANSYS/FLOTRAN was used to investigate diffuser elements for valve-less pumps. The diffuser element is a small angle flow channel with a rounded inlet and preferably a sharp outlet. It is used in the valve-less diffuser pump. ANSYS/FLOTRAN helps to visualize the fluidic flow and shows the flow directing capabilities of the diffuser element. Both two- and three dimensional models are tested and both laminar and turbulent flow models are used. It estimates the size of the flow directing efficiency but further work is needed to precisely determine the flow-pressure characteristics. The nozzle element is a wide-angle flow channel with sharp inlet and outlet. It is used in the micropump with dynamic passive-valves. There are various reasons for the direction dependence of flow resistance for the diffuser element and nozzle element. The diffuser element takes advantage of the pressure recovery in the diffuser and has the diverging-wall direction, the diffuser direction, as the positive flow direction. The nozzle element relies on the ”vena-contracta” effect and has the converging-wall direction, the nozzle direction, as the positive direction.

Paper 8

A lumped-mass model was developed especially for valve-less diffuser pumps. It was implemented using MATLAB. The model was tested for several diffuser pumps and shows good agreement with the experimental results. The flow-pressure characteristics is predicted for different excitation levels. The model makes it possible to study flows and pressures inside the pumps and shows that the maximum excitation level probably is limited of low chamber pressure. Modified designs are tested and it is shown that a pump with two serial connected pump chambers working in anti-phase is advantageous compared with a single chamber pump for both the maximum volume flow and maximum pressure head. The simulations also indicates that scaling down the diffuser elements to from 80×80 μm throat cross-sectional area to 40×40 μm throat cross-sectional area probably increase the attainable pressure head.

8 Discussion and conclusion

During this work the first micromachined pumps based on the new valve-less diffuser pump principle have been studied. The work has proved that the principle is useful for pumps with diffuser throat dimensions in the range of 30 µm (paper 2) to 3 mm [54] for different cross sectional geometries. The results indicate that that a rectangular cross-section is better than a half-elliptic cross-section.

The valve-less diffuser pump can be designed for liquid pumping for a wide range of maximum volume flows. During this work pumps have been tested with maximum volume flows in the range from 42 µl/min up to 16 ml/min and a maximum flow rate of 1.8 l/min has been reported for a bigger pump [54]. Smaller flows is possible to achieve by controlling the excitation level. The different pumps have shown different maximum pressure heads with a maximum measured pressure head of 74 kPa. The work has clearly shown that the diffuser geometry is important for the achievable volume flows and pressure heads. A simple analytic model was developed to predict the resonance frequency and the volume flow of the diffuser pump and a lumped-mass model was developed for numerical simulations of diffuser pumps. Results from simulations indicates that low chamber pressure probably is a limiting parameter for the possible maximum excitation level. That has to be considered for reliable pumping. The simulations shows that a serial pump with the chambers operated in anti-phase should be advantageous for both attainable pressure head and maximum volume flow. A reduction of the size of the diffuser elements down to 40×40 μm^2 cross-sectional throat area may also improve the pressure head.

The valve-less diffuser pump principle is useful for gas pumping. One pump designed for gas pumping was fabricated and tested. A theoretical model based on an electric analogy was developed for the gas pump.

Pumps have been fabricated using different fabrication methods and materials. Conventional fabrication methods using metal have been shown useful for fabrication of single units of diffuser pumps with good performance. Silicon micromachining using deep reactive ion etching proved to be a straightforward manufacturing method that resulted in pumps that showed the highest attainable pressure heads. Thermoplastic replication proved to be a useful method well suited for MST but it is less suited for the valve-less diffuser pump due to the flexibility of the polycarbonate.

The valve-less diffuser pump is a device with simple geometry, but with very complicated dynamic fluid behavior which is very difficult to model. This work has showed some of the possibilities of the valve-less diffuser pump and increased understanding of its function. However, still more research is needed to fully understand why and how the pump works and how to optimize it.

9 Outlook

Today microfluidics is a topic in the front-line of research activities. There is increasing demand for better devices, among them better micropumps. Different micropumps have different advantages and drawbacks. The valve-less diffuser pump has a very straightforward fabrication process and the simple geometry makes it feasible to fabricate using different material and methods depending on the application. Thermoplastic replication has the advantage of low cost and micromachined silicon/glass has the advantage of being resistant to many aggressive media. The absence of movable valves eliminates the risk of wear and fatigue in the valve and reduces the risk of valve clogging. For applications which require stationary blocking of backflow an external valve can be added. This can be either active or passive with a long time constant compared with the pump operation frequency. In this way the problem of wear and fatigue of the valve can be avoided.

The diffuser design is important for pump performance. Further work is needed to optimize the diffuser elements. This can be done using both experiments and numerical simulations. A very interesting experiment, which unfortunately seems to be difficult, is to do dynamic measurements of the diffuser characteristics. Numerical simulations that better predict the diffuser element's characteristic may be done using computers that are more powerful and a more powerful CFD-program than ANSYS/FLOTRAN. Together with a theoretical expression for the pump system, this can help to optimize the complete pump and to determine which parameters limit pump performance. The goal is then to design a reliable valve-less diffuser pump, preferably self-filling. However, the self-filling ability requires that the same pump work for both gas and liquid and consequently the excitation frequency probably needs to be changed during operation.

The valve-less diffuser pump has been shown to work as a gas pump but further studies should also make it possible to improve its gas pumping performance. The gas pump requires small dead volumes. This problem is closely connected to designing a self-filling liquid pump.

10 Acknowledgments

The work in this thesis has been carried out at the Instrumentation Laboratory, Department of Signals, Sensors and Systems, Royal Institute of Technology, Stockholm, Sweden. Financial support has been received from The Swedish National Board for Industrial and Technical Development (NUTEK) and from the Volvo Research Foundation.

Many persons have been involved in this work and I am very grateful for their help.

First of all, I want to thank my supervisors Prof. Göran Stemme and Prof. Erik Stemme for support, encouragement and professional guidance. It has been a great pleasure to work with them.

My next thanks goes to Dr. Peter Enoksson who has been a part in this project. I also want to give special thanks to Mr. Kjell Norén for all his help with different mechanical and electrical set-ups and all my other current and former colleagues at the Instrumentation Laboratory for valuable help and discussion during the work. Thanks Angelica, Bengt, Calle, Edvard, Gunbritt, Hans, Niklas, Niklas, Per-Ulf, Pontus, Thierry, Thorbjörn, Ulf and Wouter.

I want to thank Olle Larsson and Johan Holm at Industrial Microelectronics Center AB, Kista, and Lennart Lundbladh and Ove Öhman at Toolex Alpha AB that did the thermoplastic replication.

I would like to thank the staff at the Semiconductor Laboratory (HLB) in KTH-Electrum, Kista, for help with the silicon processing and Mr. Dan Claesson who carried out his Master's thesis work in this project.

Special thanks is due to Alcatel CIT and Surface Technology Systems Ltd. (STS) who did the deep silicon ion etching.

I also want to thank Dr. Tadeusz Chmielewski, my supervisor during my Master's thesis work at ABB Atom, Västerås, and Dr. Ali Massih, manager of the same group at ABB Atom. They both encouraged me to continue as a graduate student. My thanks goes also to my former colleges at the dynamics group at ABB Stal AB and specially to the manager Mr. Jari Nyquist. They took care of me during my first year after my M. Sc. degree and taught me a lot. The industrial background has been valuable to me during my Ph. D.-studies.

My last thanks goes to my family for love, support and understanding and to all the different friends that have been a part of my life during the last four and a half years. Thanks!

> ”And whatever you do, whether in word or deed, do it all in the name of the Lord Jesus, giving thanks to God the Father through him.”
> *Colossians 3:17*

Stockholm, August 1998, Anders Olsson

11 References

[1] J. Söderkvist, "Is the MEMS-commercialization micromachining or system-driven," Micro System Workshop, Uppsala, Sweden, 24-25 March, 1998, pp. 23.1-23.4.

[2] P. Gravesen, J. Brandebjerg, and O. Søndergard Jensen, "Microfluidics - a review," *Journal of Micromechanics and Microengineering*, vol. 3 (1993) 168-182.

[3] M. Elwenspoek, T. S. J. Lammerink, R. Miyake, and J. H. J. Fluitman, "Towards integrated microliquid handling systems," *Journal of Micromechanics and Microengineering*, vol. 4 (1994) 227-245.

[4] F. M. White, *Fluid Mechanics*. New York: McGraw-Hill, 1986.

[5] K. E. Petersen, "Silicon as a Mechanical Material," *Proceedings of the IEEE*, vol. 70 (1982) 420-457.

[6] S. M. Sze, *VLSI Technology*, 2 ed. New York: McGraw-Hill, 1988.

[7] E. H. Klaassen, K. Petersen, J. M. Noworolski, J. Logan, N. I. Maluf, C. Storment, W. McCulley, and G. T. A. Kovacs, "Silicon fusion bonding and deep reactive ion etching; a new technology for microstructures," Transducers'95-Eurosensor IX, Stockholm, Sweden, June 25-29, 1995, pp. 556-559.

[8] S. Johansson, K. Gustavsson, and J.-Å. Schweitz, "Strength Evaluation of Field-Assisted Bond Seals between Silicon and Pyrex Glass," *Sensors and Materials*, vol. 1 (1988) 143-151.

[9] W. K. Schomburg, J. Vollmer, B. Büstgens, J. Fahrenberg, H. Hein, and W. Menz, "Microfluidic components in LIGA technique," *Journal of Micromechanics and Microengineering*, vol. 4 (1994) 186-91.

[10] B. Büstgens, W. Bacher, W. Menz, and W. K. Schomburg, "Micropump manufactured by thermoplastic molding," IEEE 7th International Workshop on Micro Electro Mechanical Systems (MEMS'94), Oiso, Japan, January 25-28, 1994, pp. 18-21.

[11] P. Dario, N. Croce, M. C. Carrozza, and G. Varallo, "A fluid handling system for a chemical microanalyzer," *Journal of Micromechanics and Microengineering*, vol. 6 (1996) 95-8.

[12] J. Döpper, M. Clemens, W. Ehrfeld, K.-P. Kämper, and H. Lehr, "Development of low-cost injection molded micropumps," the 5th International Conference on New Actuators (Actuator'96), Bremen, Germany, June 26-28, 1996, pp. 37-40.

[13] K.-P. Kämper, J. Döpper, W. Ehrfeld, and S. Oberbeck, "A Self-filling Low-cost Membrane Micropump," IEEE 11th International Workshop on Micro Electro Mechanical Systems (MEMS'98), Heidelberg, Germany, Jan. 25-29, 1998, pp. 432-437.

[14] R. G. Gilbertson and J. D. Busch, "A Survey of Micro-Actuator Technologies for Future Spacecraft Missions," Practical Robotic Interstellar Flight: Are We Ready?, New York City, August 29 - September 1, 1994.

[15] J. W. Waanders, *Piezoelectric Ceramics - Properties and Applications*, 1 ed. Eindhoven, The Netherlands: Philips Components, Marketing Communications, 1991.

[16] S. Shoji and M. Esashi, “Microflow devices and systems,” *Journal of Micromechanics and Microengineering*, vol. 4 (1994) 157-171.

[17] J. G. Smits, “Piezoelectric Micropump with Three Valves Working Peristaltically,” *Sensors and Actuators*, vol. A21-A23 (1990) 203-206.

[18] H. T. G. van Lintel, F. C. M. van den Pol, and S. Bouwstra, “A piezoelectric micropump based on micromachining in silicon,” *Sensors and Actuators*, vol. 15 (1988) 153-167.

[19] R. Zengerle, S. Kluge, M. Richter, and A. Richter, “A Bidirectional Silicon Micropump,” IEEE 8th International Workshop on Micro Electro Mechanical Systems (MEMS'95), Amsterdam, the Netherlands, Jan. 29 - Feb. 2, 1995, pp. 19-24.

[20] E. Stemme and G. Stemme, “A Valve-less Diffuser/Nozzle based Fluid Pump,” *Sensors and Actuators*, vol. A39 (1993) 159-167.

[21] C. H. Ahn and M. G. Allen, “Fluid Micropumps Based on Rotary Magnetic Actuators,” IEEE 8th International Workshop on Micro Electro Mechanical Systems (MEMS'95), Amsterdam, the Netherlands, Jan. 29-Feb. 2, 1995, pp. 408-412.

[22] H. Mizoguchi, M. Ando, T. Mizuno, T. Takagi, and N. Nakajima, “Design and fabrication of light driven micropump,” IEEE 5th International Workshop on Micro Electro Mechanical Systems (MEMS'92), Travemünde, Germany, February 4-7, 1992, pp. 31-36.

[23] F. C. M. van de Pol, H. T. G. van Lintel, M. Elwenspoek, and J. H. J. Fluitman, “A Thermopneumatic Micropump Based on Micro-engineering Techniques,” *Sensors and Actuators*, vol. A21-A23 (1990) 198-202.

[24] S. Shoji, S. Nakafawa, and M. Esashi, “Micropump and sample-injector for integrated chemical analyzing systems,” *Sensors and Actuators*, vol. A21-A23 (1990) 189-192.

[25] R. Zengerle, A. Richter, and H. Sandmaier, “A micromembrane pump with electrostatic actuation,” IEEE 5th International Workshop on Micro Electro Mechanical Systems (MEMS'92), Travemünde, Germany, February 4-7, 1992, pp. 19-24.

[26] T. S. J. Lammerink, M. Elwenspoek, and J. H. J. Fluitman, “Integrated micro-liquid dosing system,” IEEE 6th International Workshop on Micro Electro Mechanical Systems (MEMS'93), Fort Lauderdale, Florida, USA, February 7-10, 1993, pp. 254-259.

[27] T. Gerlach, “A simple micropump employing dynamic passive valves made in Si,” MICRO SYSTEM Technologies '94, Berlin, Germany, October 19-21, 1994, pp. 1025-1034.

[28] T. Gerlach, M. Schuenemann, and H. Wurmus, “A new micropump principle of the reciprocating type using pyramidic micro flow channels as passive valves,” *Journal of Micromechanics and Microengineering*, vol. 5 (1995) 199-201.

[29] T. Gerlach and H. Wurmus, “Working principle and performance of the dynamic micropump,” *Sensor and Actuators*, vol. A50 (1995) 135-140.

[30] M. Stehr, S. Messner, H. Sandmaier, and R. Zengerle, “A New Micropump with Bidirectional Fluid Transport and Selfblocking Effect,” IEEE 9th International Workshop on Micro Electro Mechanical Systems (MEMS'96), San Diego, California, USA, February 11-15, 1996, pp. 485-490.

[31] R. Linneman, P. Woias, C.-D. Senfft, and J. A. Ditterich, “A Self-priming and Bubble-tolerant Piezoelectric Silicon Micropump for Liquids and Gases,” IEEE 11th International Workshop on Micro Electro Mechanical Systems (MEMS'98), Heidelberg, Germany, Jan. 25-29, 1998, pp. 532-537.

[32] F. C. M. van de Pol, Thesis: *A pump based on micro-engineering techniques*, University of Twente, Enschede, the Netherlands, 1989

[33] L. Smith, “Micromachined nozzles fabricated with replicative method,” Micromechanics Europe 1990 (MME '90), Berlin, Germany, 26-27 November, 1990, pp. 53-57.

[34] E. Stemme and G. Stemme, “Valve-Less Fluid Pump,” Swedish Patent Appl. No. 9 300 604-7, 1993.

[35] F. K. Forster, L. Bardell, M. A. Afromowitz, N. R. Sharma, and A. Blanchard, “Design, fabrication and testing of fixed-valve micro-pumps,” Proceedings of the ASME Fluids Engineering Division ASME 1995, FED-Vol. 234, 1995 IMECE, 1995, pp. 39-44.

[36] N. Tesla, “Valvular Conduit,” United States Patent Office 1 329 559, 1920.

[37] P. W. Runstadler, F. X. Dolan, and R. C. Dean, *Diffuser data book*. Hanover, New Hampshire: Creare Inc., 1975.

[38] T. Gerlach, Thesis: *Ein neues Mikropumpen-Princip mit dynamischen passiven Ventilen*, Technical University of Ilmenau, Ilmenau, Germany, 1996

[39] J. Ulrich, H. Füller, and R. Zengerle, “Static and dynamic flow simulation of a KOH-etched micro valve,” Transducers'95-Eurosensor IX, Stockholm, Sweden, 1995, pp. 17-20.

[40] J. Ulrich, M. Stehr, and R. Zengerle, “Simulation of a bidirectional pumping microvalve using FEM,” Eurosensor X, Leuven, Belgium, Sept. 8-11, 1996, pp. 1241-1244.

[41] M. M. Athavale, H. Q. Yang, and A. J. Przekwas, “Coupled Fluid-Thermo-Structures Simulation Methodology for MEMS Applications,” Trancducers'97, Chicago, USA, June 15-19, 1997, pp. 1043-1046.

[42] G. Strang, *Introduction to applied mathematics*. Wellesley, Massachusetts, USA: Wellesley-Cambridge Press, 1986.

[43] R. D. Cook, D. S. Malkus, and M. E. Plesha, *Concepts and applications of finite element analysis*, third ed. New York: John Wiley & Sons, 1989.

[44] *ANSYS Theory Reference*, 7 ed. Houston, Pennsylvania: ANSYS, Inc., 1996.

[45] *ANSYS CFD FLOTRAN Analysis Guide Release 5.3*, 1 ed. Houston, Pennsylvania: ANSYS, Inc., 1996.

[46] H. Schlichting, *Boundary-layer theory*, 7th ed. New-York: McGraw-Hill, Inc., 1979.

[47] W. T. Thomson, *Theory of Vibration with Applications*, 2 ed. London: Unwin Hyman, 1989.

[48] “resonance,” in *Britannica Online,* Accessed 17 April 1998 *<http://www.eb.com:180/cgi-bin/g?DocF=micro/500/38.html>*, .

[49] A. Ullman, “The piezoelectric valve-less pump - performance enhancement analysis,” *Sensors and Actuators*, vol. A69 (1998) 97-105.

[50] E. Kälvesten, L. Löfdahl, and G. Stemme, “Analytical characterization of piezoresistive square-diaphragm microphone,” *Sensors and Materials*, vol. 8 (1996) 113-136.

[51] R. Zengerle and M. Richter, “Simulation of microfluid systems,” *Journal of Micromechanics and Microengineering*, vol. 4 (1994) 192-204.

[52] P. Voigt, G. Schrag, and G. Wachutka, “Electrofluidic full-system modeling of a flap valve micropump based on Kirchoffian network theory,” *Sensors and Actuators*, vol. A66 (1998) 9-14.

[53] R. L. Bardell, N. R. Sharma, F. K. Forster, M. A. Afromowitz, and R. J. Penney, “Designing High-performance Micro-pumps Based on No-moving-parts Valves,” Microelectromechanical Systems (MEMS) ASME 1997, DSC-Vol. 62/HTD-Vol. 354, 1997, pp. 47-53.

[54] E. Stemme and G. Stemme, “A novel valve-less diffuser based fluid pump,” *World Pumps* (April 1994) 24-27, No. 331.